Geodetic and Seismic Constraints on some Seismogenic Zone Processes in Costa Rica

Edmundo Norabuena, Timothy H. Dixon
University of Miami, Rosenstiel School of Marine and Atmospheric Sciences

Susan Schwartz, Heather DeShon
Earth Sciences and IGPP, University of California, Santa Cruz

Marino Protti
OVSICORI-UNA

LeRoy Dorman
University of California, San Diego, Scripps Institution of Oceanography

Ernst R. Flueh
IFM-GEOMAR, Leibniz Institut for Marine Sciences, Kiel
and SFB574 of CAU, Kiel

Victor Gonzalez
OVSICORI-UNA

Paul Lundgren
Jet Propulsion Laboratory, California Institute of Technology

Andrew Newman[1]
Los Alamos National Laboratory

Fred Pollitz
US Geological Survey

Dan Sampson
University of California, Santa Cruz

1. Previously at *University of California, Santa Cruz*

Revised version to be submitted to *Journal of Geophysical Research*

May 15, 2004

Abstract. We report results from joint seismic and geodetic studies of the seismogenic zone in Costa Rica, where the Cocos plate subducts beneath the Caribbean plate and Panama block. Seismic data are from two combined land and OBS (ocean bottom seismometer) deployments, one in and around the Nicoya peninsula in northern Costa Rica and one near the Osa peninsula in southern Costa Rica. In the Nicoya region, inversion of GPS data suggests two locked patches centered at 14±2 and 39±6 km depth. Interplate microseismicity is concentrated in the more freely slipping region between these locked patches. This suggests that interplate microseismicity during the interseismic period does not accurately outline the up-dip limit of the seismogenic zone, the rupture zone for future large earthquakes, at least over the short (~1 year) period of our seismic observations. We also estimate northeast motion of a coastal "sliver block" at 8±3 mm/yr, probably related to oblique convergence. In the Osa region to the south, convergence is orthogonal to the trench. Cocos-Caribbean relative motion is partitioned here, with ~8 cm/yr on the Cocos-Panama block boundary (including a component of permanent shortening across the Fila Costena fold and thrust belt) and ~1cm/yr on the Panama block-Caribbean boundary. The GPS data suggest that the Cocos plate-Panama block boundary is completely locked from ~10-50 km depth. This large zone of locked slip, as well as associated fore-arc and back-arc deformation, may be related to subduction of the shallow Cocos Ridge and/or younger lithosphere compared to the Nicoya region, with consequent higher coupling and compressive stress in the direction of plate convergence.

1. INTRODUCTION

Subduction zones generate Earth's largest and most destructive earthquakes, and most tsunamis. The earthquakes result from mechanical coupling between underthrusting and overriding plates along the shallow (<50 km depth) portion of a dipping plate interface, accumulation of elastic strain during the interseismic period, and rapid release during an earthquake. Factors affecting coupling and the strain accumulation/release process are important for assessing and understanding seismic and tsunami hazard, for understanding the earthquake process, and for understanding longer term geological processes that presumably relate to subduction, such as orogeny, crustal shortening and trench-parallel

translation of fore-arc blocks (terrane migration). Key factors include the efficiency of strain accumulation (locking versus aseismic slip on the plate interface), spatial variations (up-dip and down-dip limits, along-strike variability) and temporal variation, including changing patterns of strain accumulation during the interseismic part of the earthquake cycle, and rapid seismic versus slow aseismic strain release during and shortly after the co-seismic part of the cycle.

During the interseismic period, patterns of strain accumulation on the plate interface may be determined from geodetic data, while the up- and down-dip limits of the seismogenic zone and its overall geometry may be determined from microseismicity. However, interpretations of geodetic data are non-unique, while microseismicity may not adequately delineate the main plate interface and may also exhibit temporal variation, such that short (several year) observation periods yield temporally aliased results. Earthquakes may also be poorly located if local recording stations are limited. Comparison of results from each technique is therefore useful. In this paper we describe results of joint geodetic and seismic observations, part of a large international project we have termed CRSEIZE (Costa Rica Seismogenic Zone Experiment). The observations are designed to elucidate the geometry of the seismogenic zone as well as spatial variations in locking on the plate interface in Costa Rica. Geodetically determined locked and slipping zones on the plate interface are compared with interplate microseismicity ("interseismic earthquakes") and the aftershock regions of past large earthquakes to better understand the mechanical behavior of the plate interface. We also address possible relations between short-term strain accumulation and longer-term geological processes in the subduction environment. We focus on the Osa and Nicoya peninsulas in southern and northern Costa Rica, respectively, along the Middle America Trench (Figure 1). These peninsulas enable deployment of GPS and seismic equipment quite close to the trench, immediately above much of the seismogenic zone, a situation that is quite advantageous for monitoring subduction zone seismicity and strain accumulation. The Costa Rica subduction zone is also a potential target for the Integrated Ocean Drilling Program, to drill into and instrument the seismogenic zone.

2. TECTONIC SETTING

Figure 1 shows the major tectonic features of the experiment area. The Cocos plate subducts beneath Central America, the leading edge of the Caribbean plate, at rates of about 8-9 cm/yr [*DeMets et al.*, 1990, 1994; *Dixon*, 1993; *DeMets*, 2001]. The age of subducted oceanic lithosphere ranges from ~ 15-16 Ma in southern Costa Rica to 22-24 Ma in northern Costa Rica [*Barkhausen*, 2001]. Lithosphere off southern and central Costa Rica was created at the Cocos-Nazca spreading center, and has generally rough bathymetery, while lithosphere off northern Costa Rica was created at the East Pacific Rise, and is characterized by relatively smooth bathymetry and thicker sediment cover [e.g., *Von Huene et al*., 1995; *Protti et al.*, 1995b].

There are significant contrasts in geologic characteristics of northern and southern Costa Rica that relate primarily to the age of subducted lithosphere, subduction obliquity, and the presence of absence of anomalous bathymetry on the subducted plate (Figure 2). In southern Costa Rica, the subduction direction that is essentially orthogonal to the trench, and the Cocos Ridge, an aseismic ridge created at the Galapagos hot spot, subducts beneath the Osa Peninsula. Combined with the young age of subducting lithosphere here, this results in relatively high buoyancy of the subducting slab and a shallow dipping subduction zone. This probably causes or at least influences a number of geologic features in southern Costa Rica, including lack of active arc volcanism, elevation of the Cordillera Talamanca, and back arc shortening along the North Panama deformed belt (NPDB, Figure 1), leading to development of a separate Panama block. While this block's northern boundary (the NPDB) is well-defined, its western boundary in Central Costa Rica is not well defined and may be diffuse. In northern Costa Rica, subduction angle is steeper relative to the south and an active volcanic arc is present. All or part of the Nicoya Peninsula may move as a separate block essentially parallel to the trench, associated with significant change in the trend of the Middle America trench and consequent oblique convergence [*Lundgren et al*., 1999; *McCaffrey*, 2001].

3. SEISMIC OBSERVATIONS AND RESULTS

Given geometry of typical subduction zones, accurate earthquake location may require simultaneous recording of events on land, over the down-dip portion, as well as on the sea floor, near the trench and up-dip portion. We conducted two seismic

campaigns during CRSEIZE, one near the Osa peninsula in southern Costa Rica, and the other on and offshore the Nicoya peninsula in northern Costa Rica (Figure 2). Each campaign included deployment of standard IRIS/PASSCAL three-component broadband as well as short-period seismometers on land, and three-component broadband ocean bottom seismometers (OBS) (improved versions of those described in *Sauter et al.* [1990] and *Jacobsen et al.* [1991]) as well as ocean bottom hydrophones (OBH) offshore, with extensive periods of simultaneous observations. Data from two 6-month deployments comprising 23 OBH and 15 short period land stations each between the Osa and Nicoya peninsulas, operated by SFB 574 of Christian-Albrechts Universitat Kiel and GEOMAR, comprise a total of nearly 10,000 events and are currently being processed. Results and analytical techniques for the US OBS and PASSCAL deployments are given in *Newman et al.* [2002] and *DeShon et al.* [2003a,b] and summarized here.

The OBS network originally planned for deployment directly offshore the Osa peninsula to coincide with the existing GPS transect (Figure 3) was moved 30 km northwest to take advantage of aftershocks from the August 20, 1999 M_w=6.9 underthrusting earthquake near Quepos (Figure 2a). Fourteen OBS were deployed by GEOMAR's cruise with F/S Sonne during leg S0144-1a of the Paganini expedition (San Diego-Punta Caldera) northwest of Osa between September 7-27; 1999 [*Bialas et al.*, 1999]). Twelve OBS remained operational throughout the Osa deployment. The stations were recovered, serviced and redeployed offshore Nicoya by Sonne on leg SO144-3b between December 3-19, 1999 (Punta Caldera-Balboa). The Nicoya OBS deployment covered a broad area from very near-shore to oceanic crust just seaward of the trench. Thirteen OBS remained operational throughout the Nicoya deployment until their recovery by SIO's R/V Melville on cruise NEM004 (Punto Caldera-San Diego) between June 12-28, 2000.

During the Osa OBS deployment, six land seismometers (one broadband Streickeisen STS-2 and five short period 3-component instruments) were installed along the Pacific coastline (Figure 2a). All the land stations were operating by September 24, 1999, when most of the OBS were running, and operated through November 25, 1999. The land stations were then re-deployed to Nicoya to coincide with the OBS re-deployment. During this period, a total of20 land stations were installed: 10 broadband (5 Streickeisen

STS-2, 4 Guralp 3T, 1 Guralp 40T) and 10 short-period instruments. These were distributed throughout the Nicoya peninsula in mid-December 1999 and operated through June 2001(Figure 2b).

3.1. Osa Seismic Data. The Osa array primarily recorded aftershocks of the August 20, 1999 earthquake, illuminating most of the seismogenic zone northwest of the Osa Peninsula along the northern flank of the subducting Cocos Ridge (Figure 2a). The network recorded more than 1300 regional and local events from mid-September 1999 through early December 1999. *DeShon et al*. [2003a] describe processing techniques and details of the seismic deployment and data interpretation. The main results include high precision absolute and relative relocations of aftershock seismicity that define a 19^{o} dipping plane, interpreted as the Cocos plate-Panama block interface and consistent with wide-angle refraction data for this region [*Stavenhagen et al*., 1998]. The up-dip limit of the aftershocks occurs at ~10 km depth below sea level, and the down-dip limit at 30-35 km depth, corresponding to 30-35 km and ~95 km from the trench axis respectively (Figure 2a). Aftershocks correlate spatially with the down-dip extension of the Quepos Plateau, a bathymetric high on the incoming Cocos Plate, and may reflect the structure of the mainshock rupture asperity [*Bilek et al.,* 2003]. Since the geodetic and seismic data for the Osa region are not spatially coincident, the fault plane used for geodetic models cannot be defined solely on the basis of microseismicity, although they provide a useful constraint. Seismic reflection and refraction data exist for the crest of the Cocos Ridge from seaward of the trench to the Osa peninsula coast [*Walther*, 2003], but there are no reflection or refraction seismic data tracing the plate interface beneath the peninsula itself.

3.2. Nicoya Seismic Data. The Nicoya network imaged the Middle America subduction zone offshore northern Costa Rica from seaward of the trench, across the entire Nicoya Peninsula, through to the Nicoya Gulf (Figure 2b), recording more than 8000 regional and local earthquakes from December 1999-June 2001. Experiment details and hypocenter locations obtained with a fixed velocity model are described in *Newman et al.* [2002]. Shallow seismicity beneath the Nicoya Peninsula, both crustal and along the plate interface, represents about 20% of the earthquakes located by *Newman et al.*

[2002]. Data analysis originally focused on the July 21, 2000 M_w 6.4 outer-rise earthquake and its aftershocks (Figure 2b). This event was a normal faulting earthquake that ruptured the oceanic crust and possibly into the mantle in the vicinity of the Fisher Seamount Chain [*Schwartz et al.,* 2001]. Pertinent results from this work include observation of deep slab seismicity extending down to 220 km, recorded but not well-constrained by the Nicoya network, a large number of well-located interplate and intraplate events shallower than 50 km, and variability in the depth of the shallowest seismogenic zone earthquakes, possibly corresponding to differences in subducted oceanic crust and regional heat flow patterns [*Langseth and Silver*, 1996; *Harris and Wang,* 2002; *Fisher et al*., 2003; *Walther and Flueh*, 2002].

DeShon et al. [2003b] relocated earthquakes analyzed to date (almost twice as many events as included in our earlier study [*Newman et al.*, 2002]) using a simultaneous inversion for a minimum one-dimensional P- and S-wave velocity model, Nicoya network station corrections, and earthquake locations. The updated Nicoya hypcenters (Figures 2b,c) are similar to those obtained by *Newman et al.* [2002]. The depths of some of the earthquakes are a few km shallower due to differences in the shallow velocity model used for earthquake location. Figure 2b also shows a subset of well-located events (673 events, rms < 0.10 seconds) with a location precision (one standard error) better than 1 km in both horizontal and vertical components.

One important application of our precise earthquake locations is the geometric definition of the plate boundary for modeling the geodetic data (mis-location of the plate interface may introduce systematic error in strain accumulation models). Figure 2c is a cross section of the Nicoya portion of the plate boundary, showing the model plate interface and supporting data. The shallow (< 25 km) plate boundary is clearly identified from seismic reflection and refraction data along profile S-S' (Figure 1). The locations of the subset of well-located events whose hypocenters lie within 20 km of S-S' are also shown. While there may be slight variations in slab dip along strike beneath Nicoya, a composite surface composed of three planar segments, whose dip increases with depth, fits the reflection/refraction data and the overall pattern of seismicity quite well. From the trench axis (~5 km below mean sea level, the datum for all depths reported here) the shallow plane of the model surface closely follows that defined by seismic reflection and

refraction, dipping at 10° to a depth of 15 km. From 15-38 km depth, the intermediate model surface dips at 25°, through a group of hypocenters that delineate a well-defined plane. Beneath 38 km, the dip of the model plane increases to 43° to project through the center of a loose cluster of events between 40 and 60 km depth (the reduced number of events below ~ 50 km depth reflects not only the transition to more ductile conditions at depth, but also reduced sensitivity of our array to the deeper plate interface). We interpret a cluster of shallow events in the cross section above the model plane at 10-15 km depth (about 80 km from the trench axis) as upper plate events. We estimate location accuracy (one standard error) of the model plane to be ±2km above 15 km, and ±5 km beneath 15 km. As described below, this uncertainty has a negligible influence on the geodetic model results.

4. GEODETIC OBSERVATIONS

Lundgren et al. [1999] reported velocities from a geodetic network of 23 GPS sites in Costa Rica first measured in 1994 (Figure 3). To improve the accuracy of the site velocity estimates, we resurveyed this network in January-February 2000 using Trimble SSI receivers with Dorn-Margolin antennas and "choke ring" backplanes, extending most time series by three years with observations of 3-5 days at most sites. We also installed and made first epoch position measurements on 20 new sites in Costa Rica (Figure 3). Data were analyzed with techniques described in *Sella et al.* [2002]. Table 1 lists site locations, velocities for all sites with at least two occupations of a campaign site separated by at least three years, or more than 2 years of data for a continuous site, in reference frame ITRF-97 [*Boucher et al.,* 1999], and uncertainties (unless noted, all uncertainties in the text and tables represent one standard error, while velocity error ellipses in figures represent two-dimensional 95% confidence regions). Table 2 lists data quantity and weighted rms (wrms) scatter about a best fit line through the daily position estimates, a measure of data quality. Velocity error estimates include the effects of "colored" (time-correlated) noise [*Mao et al.,* 1999; *Dixon et al.,* 2000]. Our vertical velocities are still too imprecise to provide meaningful model constraints (Tables 1 and 3). Vertical site velocities are listed in Table 1 but not used in the subsequent models or discussion.

The wrms scatter of these data (Table 2) is somewhat higher compared to other data with similar observing times and analytical techniques obtained by our group in western North America [e.g., *Dixon et al.*, 2000, 2002]. This may reflect the high and variable wet tropospheric path delay experienced by the microwave GPS signals in the tropical Costa Rica environment (8°-11°N latitude) [*Dixon and Kornreich Wolf*, 1990], compared to the drier conditions for the cited North American studies (30°- 40°N latitude). *Mao et al.* [1999] noted a relation between absolute latitude and noise in GPS velocity estimates, and discussed the possible influence of the tropical troposphere. The larger data set in *Sella et al.* [2002] shows a clear relation between latitude and wrms scatter, especially for the vertical component. This component is quite sensitive to mismodelling of the atmosphere, consistent with the idea that tropical tropospheric effects contribute to higher noise levels of the Costa Rican GPS data. Our model for estimating GPS site velocity uncertainty incorporates these effects to first order, hence geophysical model parameters derived using weighted least squares techniques should not be significantly biased by these higher noise levels.

Table 3 and Figure 3 give horizontal site velocities relative to the Caribbean plate, as defined by *Sella et al*. [2002]. Figure 3 also shows the overall plate convergence direction, using the Cocos-Caribbean angular velocity vector of *DeMets* [2001] based on geologic data. This model agrees well with the single available measurement of present day plate motion here (from GPS), 88 mm/yr at an azimuth of 022°, derived from a baseline that crosses the trench at 8.7°N, between Cocos Island (the only point of land on the Cocos plate) and San Andres Island on the stable interior of the Caribbean plate [*Dixon*, 1993] (calculated at the same position, the geologic vector is 89 mm/yr at an azimuth of 024°). While the convergence rate at some other subduction plate boundaries has apparently slowed since Pliocene time [e.g., *Norabuena et al.*, 1999], the close agreement here between the geodetic measurement averaged over a few years and the corresponding geologic value averaged over several million years indicates remarkably steady convergence, in contrast to the argument of *Murdoch* [2003] that Cocos-Caribbean convergence has recently slowed.

In the Caribbean plate reference frame, site velocities on or near the Caribbean coast that lie on the Panama block can be expected to have residual motion relative to the Caribbean plate, while coastal Caribbean sites to the north, not on the Panama block, should have essentially zero residual motion. Eventually this velocity differential should allow accurate identification of the northern boundary of the Panama block in central Costa Rica, although the current data set is too sparse. From Figure 3, it is apparent that the velocity field in southern Costa Rica is essentially parallel to plate motion, mainly reflecting elastic strain accumulation on the locked plate interface [e.g., *Savage*, 1983]. In contrast, the velocity field in northern Costa Rica in the vicinity of the Nicoya peninsula displays a distinct rotation of vectors relative to the plate convergence direction, suggesting the influence of one or more additional processes. These processes need to be considered before interpreting the GPS data in terms of strain accumulation on the plate interface.

5. MODELING THE GEODETIC DATA

The surface velocity field measured by GPS represents the integrated effect of a variety of short-term elastic (recoverable) deformation processes and longer-term processes that may permanently deform the upper plate. In order to use the geodetic data to study these processes, we require a model that adequately represents all the significant effects, i.e., those that contribute signal at or above the noise level of the observations, roughly 1-2 mm/yr in horizontal components. This requires some assumptions and simplifications, and consideration of available geologic and seismic constraints. We approximate the complex rheological structure of the region with a simplified rheology, described below, and consider five processes:

1. Elastic strain accumulation in the upper plate due to a locked or partly locked plate interface;

2. Post-seismic response to major past earthquakes;

3. Trench-parallel motion of a fore-arc block due to oblique convergence;

4. Shortening on out-of-sequence (non-plate boundary) thrust faults and folds in the fore-arc region;

5. Deformation in the back-arc region.

We assume that processes 1 and 2 result in no long-term deformation of the upper plate. Process 3, while it does involve (or likely involves) elastic deformation, ultimately results in permanent deformation of the upper plate, at rates that may be significant on geodetic time scales. Similarly process 4 may involve elastic deformation on out-of-sequence thrust faults, but ultimately results in permanent shortening of the upper plate. Process 5 may involve both permanent shortening on out-of-sequence thrusts and elastic deformation associated with temporarily locked motion on the Caribbean plate - Panama block boundary, analogous to Process 1. For clarity, recall that shortening across a subduction zone as measured by GPS, e.g., between mainland Costa Rica and the center of the Cocos plate [*Dixon*, 1993], represents plate convergence and in that sense is permanent. However, the resultant shortening of the upper plate is mainly elastic, reflecting temporary locking on the main plate boundary thrust that will be released in the next large earthquake. The associated compressive stresses may also drive a small component of permanent deformation (shortening) on nearby out-of-sequence thrusts in the fore-arc, as evidenced by geologic data, typically a small fraction of the long term plate convergence rate and often a fraction of the maximum elastic shortening in the upper plate [e.g., *Norabuena et al.*, 1998; *Nicol and Beavan*, 2003]. Similar reasoning applies to motion between the Panama block and the Caribbean plate. In general, separating elastic and permanent shortening may be difficult if the plate boundary and out-of sequence thrusts are closely spaced, so independent geological information is usually required.

We also assume that process interactions can be ignored, and the measured velocity field reflects the linear superposition of these five processes. Hence their effects can be calculated separately and summed. To further simplify our problem, we split the data set into a southern (Osa) section and a northern (Nicoya) section (there is very little data for central Costa Rica at present). As discussed below, the southern section is affected by processes 1,2,4 and 5, while the northern section is affected mainly by processes 1, 2 and 3. Other assumptions and simplifications are described below, as well as a summary of available data constraints.

5.1 Elastic Strain Accumulation from a Locked Plate Boundary. The dominant process affecting the surface velocity field in the region, and the primary focus of this paper, is interseismic strain accumulation associated with a locked subduction zone plate interface. Over time, earthquakes periodically release accumulated strain, accommodating relative motion between the Cocos and Caribbean plates and the Panama block. The degree of mechanical coupling between the plates (the amount of long term plate motion or "slip" that is temporarily locked on the plate interface during the interseismic period) affects the rate of strain accumulation. Geodetic subduction zone studies usually report "locked slip" or "backslip" [*Savage*, 1983] on the plate boundary fault rather than "creep rate", and we follow that convention here; locked slip equal to the full plate or block convergence rate, corrected for shortening on nearby out-of-sequence thrusts, implies a creep rate of zero.

Lundgren et al. [1999] presented the first estimates of spatially variable locked slip on the Costa Rica plate interface, and demonstrated significant spatial variation. The improved data set allows us to refine this picture considerably. We assume that strain accumulation can be modeled as a perfectly elastic process, i.e., strain accumulated in the interseismic period is completely released during the subsequent major earthquake, with no permanent deformation of the upper plate. We use the method of *Pollitz et al.* [1998] to investigate the amount of locking and its spatial variation on the seismogenic plate interface, using a constrained inversion of the surface velocity field. Site velocities are inverted to obtain the slip distribution $s_j(x,y)$ (locked slip) on rectangular fault planes with index *j*. The slip distribution is parameterized using a set of smooth basis functions (Hermite-Gaussian functions as defined in *Pollitz et al*. [1998]. The maximum likelihood solution is obtained by minimizing a penalty function β:

$$\beta^2 = \chi^2 + \mu\Sigma_j|\Delta s_j(x,y)|^2$$

where χ^2 is the data misfit (sum of squared residuals normalized by error squared) and $|\Delta s_j(x,y)|^2$ (smoothness) is a measure of the stability of $s_j(x,y)$, controlled by the damping factor μ.

For Osa, where other relevant data are limited, we approximate the plate interface as a single plane whose long axis is oriented parallel to the mean strike of the trench direction,

and vary the dip for best fit. For Nicoya, where our new seismic data plus existing refraction data provide significant constraint (section 2), we approximate the plate interface as three adjacent planes, with long axes parallel to the mean trench direction, whose dip increases with depth (Figure 2c). To avoid edge effects we extend the planes 150 km beyond the study region, defined by data availability. A given fault plane is parameterized with 120 mutually orthogonal basis functions, so that 120 degrees of freedom per fault plane are available to describe its slip distribution. We impose the constraint that slip at every location on the plane is parallel to the local plate motion; the inversion then gives the amplitude of the slip distribution.

Most models assumed a depth extent of the seismogenic plate boundary from 0-50 km. To investigate the sensitivity of results to these up-dip and down-dip boundary conditions, we also tested models with a minimum depth of 15 km, and maximum depths of 42 and 60 km.

Since 120 parameters for a given fault plane greatly exceed the number of data, the inversion is constrained ("damped") to avoid solutions with too many degrees of freedom, and the amount of locked slip on any given patch can vary only slightly from its neighbors (without such constraints, we could obtain essentially perfect fits to the data, but the solutions would not be meaningful). We performed numerical tests to investigate the trade-off between misfit (χ^2) and damping (μ) to find a reasonable value. Figure 4 shows a typical trade-off curve. We did not directly constrain the inversion results to have upper or lower bounds, i.e., the amount of locked slip could exceed the plate rate, or could have negative values. However, since values beyond the plate rate and negative values are physically implausible, we did use these criteria to constrain appropriate damping factors, limiting such extreme values to a small percentage of the overall fault area.

We also performed "checkerboard" tests (Figure 5) to assess the ability of the data to resolve spatial variations in locking for the Nicoya region, where spatial density of GPS sites is relatively high (at present we have much less resolving power for the Osa region due to limited data). First, we assigned contrasting patterns of slip to the fault plane, representing respectively locked and freely slipping patches. Next, we computed the resulting surface displacement at the locations of the GPS sites, and assigned Gaussian

noise at the level of 10% of site velocity. We then inverted this synthetic data set using the damping values derived above, solving for slip on the fault plane. Blocks of the size shown in Figure 5 (30 by 40 km) are reasonably well resolved. While there is some "smearing" (the sharp boundary between locked and slipping patches in the synthetic input data is smoothed by the inversion), it is clear that locked patches of the size and location shown can be resolved, and their locations accurately recorded, even if located offshore. Even the up-dip edge of the synthetic locked patch, 25-35 km offshore, is reasonably well-resolved.

Before inverting the data to estimate the distribution of locked slip on the plate boundary, we first account for other processes affecting the velocity field, as described below.

5.2 Post-Seismic Motion. Large earthquakes stimulate viscous flow in the lower crust and upper mantle, which in turn affects the surface velocity field via tractions on the upper crust. Post-seismic response to smaller events or events far in the past is small and can be ignored. We initially considered the four largest earthquakes in the region in the last 20 years (Table 4), and used the model of *Pollitz* [1997] to estimate corresponding surface displacements during the time frame of GPS observations. Of the four earthquakes considered, only two (1991 Valle de Estrella earthquake in the Osa back-arc region, 1992 Nicaragua earthquake) produced significant displacement at the GPS sites during the observation period for the range of tested rheological models, described below. The calculated post-seismic response from these two events is used to "correct" the velocity field prior to estimation of other parameters, as described in the Results section.

While the rheologic structure strongly influences the computed post-seismic response, our data are insufficient to invert directly for rheology. Instead, we define a limited number of plausible models based on other information, and use these to compute a series of forward models. Our rheological model consists of three layers in a radially symmetric earth: an elastic upper crust to a depth of 16 km, a Maxwell viscoelastic lower crust to a depth of 30 km, and a Maxwell viscoelastic mantle. *James et al.* [2000] define the rheology of the upper mantle in the Cascadia subduction zone, using Holocene relative sea level data describing the regional history of post-glacial rebound. They infer

a mean upper mantle viscosity of 10^{19} Pa-s, considerably smaller than values for the interior of North America based on glacial isostatic adjustment (10^{20}-10^{21} Pa-s; e.g., *Peltier* [1998]). This probably reflects the addition of water to the upper mantle during subduction [e.g., *Peacock*, 1993], which significantly weakens olivine rheology [*Kohlstedt et al.*, 1995; *Hirth and Kohlstedt*, 1996], perhaps to the point where the uppermost mantle here has lower effective viscosity than the lower crust. We tested values of lower crust and upper mantle viscosity of 10^{18}, 10^{19} and 10^{20} Pa-s, for a total of 9 rheological models (3 lower crustal values x 3 upper mantle values).

5.3. Trench-parallel motion of a fore-arc "sliver" block. Many subduction zones experience oblique convergence, where the trench-normal direction differs from the plate convergence direction. Trench-parallel motion of fore-arc crustal blocks in response to the resulting shear stress is an important aspect of crustal deformation [*Fitch*, 1972; *Jarrard*, 1986], results in permanent deformation of the upper plate, and may be an important mechanism for generation of "exotic terranes" in the western parts of North and South America.

Parts of Central America experience northwest translation of coastal regions due to oblique convergence [*DeMets*, 2001; *McCaffrey*, 2002]. Motion of these blocks, located between the trench and the volcanic arc, is likely to be significant in areas of rapid subduction and high obliquity, especially where young lithosphere is subducted and mechanical coupling between subducting and overriding plates is likely to be high [*Beck*, 1991; *McCaffrey*, 1992]. In Central America, obliquity varies due primarily to changes in the trend of the trench. Using new compilations of bathymetric data [*Ranero and von Huene*, 2000] and the plate motion model of *DeMets* [2001] we computed subduction obliquity for the Middle America Trench offshore Costa Rica (Figure 6). Obliquity varies from essentially zero (i.e., orthogonal subduction) in southern and central Costa Rica to about 20° in the northern and central Nicoya peninsula. Although slip vector azimuths of plate boundary earthquakes appear to be rotated clockwise from the plate convergence direction in the Nicoya region (latitude range ~ 9-10.5°N), consistent with northwest block motion in response to oblique subduction, there is considerable scatter in the data, and a precise estimate of block translation rate from these data is not possible.

DeMets [2001] calculated 14±2 mm/yr of northwest fore-arc motion relative to the Caribbean plate in the Nicaragua segment of the arc, north of the Nicoya peninsula.

GPS vectors in the Nicoya region exhibit significant counter-clockwise rotation relative to the plate convergence direction and relative to observed directions in the Osa region, consistent with northwest translation of a sliver block in the former, and no such motion in the latter. We first compute synthetic velocity fields for various post-seismic response models (section 5.2 above), compute synthetic velocity fields for various models of sliver transport (0-16 mm/yr of northwest translation, assuming a simple elastic half space model and a single hypothetical strike slip fault through the volcanic arc that accommodates block motion, locked to a depth of 10 km), correct the observed velocity field for both model processes to derive a residual field that mainly reflects elastic strain accumulation on the plate boundary, and invert this residual field as described in section 5.1. The process is repeated for all possible model combinations, defining a series of satisfactory (low-misfit) models. The models are non-unique, because various combinations of parameters may yield similar low-misfit models that are statistically indistinguishable. We can nevertheless define an acceptable range of models, generating an estimate of block translation rate and its uncertainty.

5.4. Fore-arc shortening. In southern Costa Rica, long term shortening is accommodated within the Fila Costena on the Pacific coast. *Fisher et al.* [2003] document a minimum of 8.7 mm/yr of average Quaternary shortening across the Fila Costena fold and thrust belt. In the discussion below, we assume a value of 1 cm/yr. Only the southern part of the GPS data set is affected by this process; similar fore-arc belts have not been identified north of about 10° N.

5.5. Back arc deformation. In southern Costa Rica, elastic and possibly permanent deformation (shortening) also occur in the back arc region, on and near the North Panama deformed belt, a fold and thrust belt marking the boundar between the Caribbean plate and the Panama block [*Case and Holcomb*, 1980; *Adamek et al.*, 1988; *Vergara-Munoz*, 1988; *Silver et al.*, 1990, 1995] (Figure 1). The 1991 M_w=7.6 Valle de Estrella earthquake was a thrust fault earthquake on a southwest-dipping fault defining the northeast corner of the belt, indicating that this boundary is active [*Plafker and Ward*, 1992; *Goes et al.*, 1993; *Lundgren et al., 1993*; *Protti and Schwartz*, 1994]. Determining

the long term angular velocity of a separate Panama block relative to the Caribbean and Cocos plates [e.g., *Sella et al.*, 2001] would be useful, but is difficult with the current sparse data set.

6. RESULTS OF GEODETIC MODELS

6.1 Osa Peninsula. The pertinent processes affecting GPS velocities in southern Costa Rica are believed to be: 1) elastic strain accumulation on the locked plate interface; 2) post-seismic response to the 1991 Valle de Estrella M_w 7.7 earthquake; 3) permanent shortening in the fore-arc ; 4) elastic and possibly permanent deformation in the back arc. We first correct the velocity field for the post-seismic response (2), then solve for plate boundary and back arc deformation (1 and 4) by estimating the amount of locked slip on two thrust faults with opposing dips in a simultaneous inversion (Figure 7). We then consider the effects of fore arc shortening (3) on the interpretation of results. GPS data in the Osa region are too sparse to reliably resolve spatially variable slip on the plate boundary. For comparison with the Nicoya results, we present a similar solution (Figure X) but only the mean locked slip (Table 5) is well-constrained.

For the 1991 earthquake we used the source model of *Plafker and Ward* [1992] to predict post-seismic motions, and subtracted them from our observations. The geometry of the Panama block-Caribbean plate boundary was based on *Protti and Schwartz* [1994], oriented with its long axis perpendicular to plate motion and dipping 20° southwest. The model plane has a sharp northwest boundary as indicated in Figure 7, but in fact this boundary is not well defined. To avoid edge effects the plane extends 150 km southeast of the study area at constant strike and dip. This agrees only approximately with geological studies, but our results are not sensitive to this aspect of the model since we have no data there. Site Limon (LIMN) is near the northwest boundary of the block [*Marshall et al.,* 2000] and hence may be sensitive to edge effects.

Overall plate convergence here (Cocos-Caribbean relative motion) can be considered partitioned between the Cocos plate-Panama block and Panama block-Caribbean plate boundaries. The inversion results suggest that the Cocos-Panama boundary is accumulating ~8 cm/yr of locked slip, while the Panama-Caribbean boundary is

accumulating ~1 cm/yr of locked slip (Table 1). The sum of these gives the total (Cocos-Caribbean) convergence, ~9 cm/yr. A patch of anomalous slip near site LIMN may reflect edge effects associated with the Panama block boundary (this is a sharp boundary in our model, but is more likely diffuse). A small patch of high locked slip on the Pacific coast (exceeding the plate rate) is probably an artifact of our limited data. The estimates of locked slip on the plate or block boundaries in the Osa region are based on a sparse data set that is essentially a transect. Hence the estimates have little validity northwest or southeast of the transect, beyond about 20-30 km on either side of the transect line.

The inversion results include elastic deformation on the main plate or block boundary as well as permanent shortening on nearby structures. For the main plate boundary, we can estimate the magnitude of this effect using available geologic data. Assuming 1 cm/yr of permanent shortening across the Fila Costena [*Fisher et al*., 2003] implies 7 cm/yr of elastic locked slip on the main Cocos-Panama boundary, to be released in a future earthquake. Analogous information is not available for the back arc region. Additional observations at all available sites (Figure 3), explicit inclusion of Fila Costena structures in the models, and a refined boundary for the Panama block, are needed to improve these results.

6.2 Nicoya Peninsula. The major processes affecting the surface velocity field in northern Costa Rica are: 1) elastic strain accumulation on the locked plate interface; 2) trench-parallel motion of the fore-arc block due to oblique convergence; and 3) post-seismic response to the 1992 Nicaragua tsunami earthquake. We first correct the velocity field for the post-seismic response, then estimate motion of the fore-arc block and patterns of locked slip on the plate interface. Since geodetic data density is much higher in the Nicoya region compared to Osa (Figure 3), we can resolve the spatial distribution of locking on the main plate interface here.

The 1992 Nicaragua earthquake had a very slow rupture, around 100 seconds, and caused a tsunami much greater than expected for its surface wave magnitude (M_s=7.2) [*Ide et al.,* 1993]. Using *Kanamori's* [1972] terminology, this event may be described as a tsunami earthquake [*Kanamori and Kikuchi*, 1993]. There are significant differences in

published estimates of rupture area for this event, which may reflect the slow rupture and corresponding differences in energy release in different frequency bands. *Satake* [1994a,b; 1995] used tide gauge data and tsunami run-up heights to invert for fault rupture, determining a relatively narrow band of co-seismic slip starting at the trench, extending 250 km parallel to the trench and 40 km down-dip. Aftershocks define a considerably larger rupture area, extending down-dip to much greater depth. This suggests that afterslip extended the total rupture area to deeper depths. Figure 8 shows the fault plane inferred from tsunami studies [*Satake*, 1994a,b] (hereafter termed the tsunami model), all aftershocks up to thirty days after the event, and our approximation of the larger fault area as a rectangular plane based on these aftershocks, hereafter termed the aftershock model, similar to the plane defined by *Ihmlé* [1996] based on 90 days of aftershocks. Both the tsunami and aftershock model fault planes are used to generate a series of post-seismic response models.

The computed post-seismic response is proportional to total moment, and hence is sensitive to fault slip for a given fault area. Estimates of the mean slip for the 1992 Nicaragua event vary by nearly an order of magnitude (e.g., 0.38 m, *Imamura et al*. [1993]; 3.0 m, *Satake* [1994] reflecting the uncertainty of the fault area and the slow rupture characteristics of this event (estimates of total moment vary less). The higher dislocation values are based on tsunami models. The post-seismic response is sensitive to the total slip, including afterslip that may have accumulated in the weeks and months following the main shock, which is not reflected in either the seismic or tsunami models. We tested models with 1.0, 3.0 and 5.0 meters of slip, and thus considered a total of 54 post-seismic response models for the 1992 event (9 rheological models x 2 fault planes x 3 mean slip values). For all tested models, the computed post-seismic response to the 1992 earthquake at the GPS sites in the middle of the observation epoch (1997) was typically less than 2 mm/yr, although the spatial patterns of deformation varied considerably.

Figure 9 plots the chi-square misfit for the ten lowest misfit models for both the aftershock and tsunami models as a function of northwest block translation rate, showing a well-defined minimum at 8±3 mm/yr.

Figure 10 shows the inferred slip distribution on the Nicoya portion of the plate boundary fault for the best-fitting (minimum chi-square) solution, and the corresponding observed and calculated velocity vector (the model velocity includes the effects of 8 mm/yr of northwest block motion and post-seismic response, as described above). The slip distribution shows two patches of locked slip, with the maximum (~6 cm/yr) centered at 14±2 km depth, and a lower one (~3 cm/yr) at 39±6 km depth, separated by a region of lower locking (~2-3 cm/yr from 22-30 km depth) centered at 24 km depth. Based on the checkerboard resolution test, these patches could either represent the gradational distribution illustrated, or perhaps two smaller, fully locked patches separated by a freely slipping region. This is better illustrated in Figure 11, where we adjust the position of two small, fully locked input patches in a checkerboard test to yield an output that roughly matches results of the data inversion. Thus the current data cannot distinguish between gradational variations in locked slip and a more abrupt pattern of locked and freely slipping zones.

The occurrence of two patches of locked slip near the up-dip and down-dip limits of the seismogenic zone is present in all of the low-misfit models for Nicoya. We tested the robustness of this result in several ways. In terms of sensitivity to post-seismic models, Figure 12 plots the amount of locked slip on the seismogenic zone as a function of depth, for the 10 lowest misfit models, for both the aftershock and tsunami models of the 1992 earthquake fault plane. Also shown is a reference line showing 50% of the plate convergence rate (4.3 cm/yr at this location). Locked slip exceeding 50% of the plate rate occurs only in a narrow depth range on the plate interface, ~11-18 km. All of the geodetic model results have locked slip that peaks at about 14 km depth, although the maximum amount of locked slip varies slightly with the various models, between about 5 and 7 cm/yr.

We tested the sensitivity of the locking pattern to possibly erroneous data at individual sites by successively eliminating a data point and re-inverting the edited data set (Figure 13). In all cases the overall pattern of two highly locked patches is retained, although the maximum and minimum amplitudes vary slightly. The largest variation is observed when data for station ZUMA is removed, but even here the key results noted above persist.

The three dimensional location of the model plate interface may also influence the estimated locking pattern. We tested the sensitivity of results to systematic errors in the location of this interface in several ways. First, we defined two other model plate interfaces, along the upper and lower surface of interplate microseismicity in the depth range 15-50 km, i.e., above and below what we believe to be the optimum interface (Figure 2c). In both cases the shallow locked patch remains, at about the same distance from the trench. We also ran a test where the uppermost fault plane was eliminated, forcing all the locked slip to be distributed on the two deeper planes. Data misfit increased significantly, regardless of rheological model, but the peak in locked slip for the shallow locked patch remained shallow, at the top of the remaining two planes. A test of the sensitivity of the deeper locked patch to the down-dip extent of the model interface suggests that results do have some sensitivity to this parameter. For example, extending the model plane from 50 km to 60 km depth reduces the peak magnitude of locked slip from 3.5 cm/yr to 2.7 cm/yr, although the general location of the deeper locked patch is not affected (Figure 15). For all tested models, the down-dip limit of locking (i.e., locked slip less than about 2 cm/yr) approximately coincides with the down-dip rupture limit of past earthquakes (Figure 17).

In summary, the overall pattern of shallow locked slip is a robust result and is not sensitive to model details. The magnitude and extent of the deeper locked patch does exhibit some sensitivity to the assumed down-dip extent of locking.

7. DISCUSSION

7.1 Up- and Down-Dip Limits of the Seismogenic Zone

The up-dip limit of the seismogenic zone is often defined on the basis of interseismic microearthquakes [e.g., *Newman et al.*, 2002; *Obana et al.*, 2003] and compared to other geophysical quantitities, e,g., thermal state, and laboratory data on the stability of different minerals as a function of pressure and temperature, in order to elucidate seismogenic processes. One of the motivations of our study was to compare the up-dip and down-dip limits of the seismogenic zone as defined from interseismic microearthquakes and geodesy. In the Nicoya region both data sets are large enough to

make this comparison rigorous. Figure 16 suggests that the microseismic and geodetic definitions of the up-dip limit do not agree, at least for the time span sampled by our data. The geodetic data show an increase in locked slip beginning about 25 km inland from the trench (~8 km depth), and a clear peak in locked slip 50 km from the trench (14 km depth), considerably up-dip from the beginning of significant microseismicity, 65km from the trench (~16 km depth). The distinctive patterns of locking and microearthquake location are well illustrated in both map view (Figure 16) and cross-section (Figure 3c); very few microearthquakes overlap the locked regions. Microearthquakes on or near the plate boundary are restricted to the more freely slipping parts, while events within the upper plate tend to concentrate near the shallow transition from locked to more freely slipping regions. The distinct nature of the geodetically and micro-seismically defined up-dip limit of the seismogenic zone is a robust result: our combination of on-shore and offshore seismometers means that the earthquakes are precisely located (horizontal uncertainties less than 1 km), while the geodetic results benefit from the dense station spacing and the fact that the Nicoya peninsula is located close to the trench, above most of the seismogenic zone, and as noted earlier are not sensitive to model details.

All acceptable models also produce a down-dip locked or partly locked patch (Figures 13,14, 15) although with less well-constrained magnitude, extent and down-dip limit compared to the shallow patch. Microearthquakes in this region are somewhat diffuse, and may not all be plate interface events (our seismic array may also have reduced sensitivity here). Therefore, we cannot rigorously assess the relation between geodetic and seismic definitions of the down-dip seismogenic limit. To a first approximation, both locking and microseismicity decrease significantly below about 50 km.

The simplest interpretation of this pattern of locking vs. microseismicity is that the shallow (10-15 km) locked patch is fully locked and does not produce significant microseismicity; below this, to a depth of ~ 40 km, the plate interface transitions from fully locked to substantially slipping and is a locus for abundant inter- and nearby intra-plate seismicity. If this pattern is generally true, it suggests that interseismic mircoearthquakes are a good way to outline the overall geometry of the plate boundary,

but do not necessarily correspond to regions of high strain accumulation, and thus cannot reliably indicate the up-dip limit of the seismogenic zone, and may not reliably indicate the down-dip limit of the seismogenic zone.

Does the up-dip locked patch correspond to the up-dip limit of a future large earthquake? Figure 17 superimposes the aftershock areas of three past large earthquakes on the pattern of locked slip for the Nicoya region. The largest event was the 1950 Nicoya earthquake (M_s=7.7); its epicentral location, along with the 1978 (M_w=7.0) Sámara earthquake were recomputed by *Avants et al.* [2001] relative to the well-located 1990 (M*w*=7.0) event [*Protti et al.,* 1995]. *Protti et al.* [2001] suggested that the 1978 earthquake could have been a compressive intraplate event on the Cocos plate, based on its location, focal depth and mechanism, reflecting bending of the oceanic plate due to a locked plate interface. However, the relocation of the 1978 event refines its depth estimate, such that its location is consistent with an interplate event. Although details of the coseismic slip distribution for the 1950 event are not known, the up-dip limit of the 1950 aftershock area appears to correspond with the up-dip edge of the locked patch.

Hyndman and Wang [1993] and *Oleskovich et al.* [1999] suggested that the up-dip limit of the seismogenic zone corresponds to the 100-150°C isotherm. Using the thermal model of *Spinelli and Saffer* [2004] we compared the up-dip locking limit and the microseismicity pattern in the Nicoya region to the location of the 100°C isotherm. This isotherm corresponds approximately to the up-dip limit of the geodetically determined locked patch (Figure 16) and the up-dip rupture limit of past large earthquakes (Figure 17). The thermal model of *Spinelli and Saffer* [2004] accounts for the abrupt difference in seafloor heat flow values obtained on East Pacific Rise (EPR) versus Cocos-Nazca Spreading Center (CNS) crust, including 1-2 km of hydrothermal cooling of the EPR crust [*Fisher et al.,* 2003]. The offset in the 100° C isotherm, coincident with the change in oceanic crustal origin, is mimicked by a slight shallowing of the up-dip edge of the geodetically locked patch (Figure 16). If we define the up-dip limit of the seismogenic zone as the shallowest region able to accumulate significant strain (and hence likely to rupture seismically in a future earthquake), rather than the shallow limit of interseismic microearthquakes, these observations suggest that the up-dip limit at this location is

controlled by thermally mediated diagenetic processes or low-grade metamorphic reactions near 100°C.

An important question to be answered by future observations is the extent to which the distribution of locked slip and microearthquakes is time-transient. Perhaps the patterns we observed would be different in different parts of the earthquake cycle.

7.2 Earthquake Cycle Deformation

Spatial variability in coseismic slip during large earthquakes has been recognized for some time; however, the nature and persistence of regions of enhanced coseismic slip (asperities) and the behavior of the intervening weaker regions from one great earthquake to another and within an earthquake cycle are still unresolved. The simplest concept, know as the characteristic earthquake model, states that an earthquake is produced when a particular portion of the fault plane (asperity) fails in seismic rupture, with a recurrence interval equal to the time required for stress at that asperity to rebuild to a given level (presumably where its failure strength is exceeded). Assuming constant tectonic loading (stress rate), and either constant failure stress (constant material properties), final stress, or both, the slip and/or the recurrence time of future large earthquakes is thus predictable. These models have served as the basis for assessing long-term earthquake potential at active plate boundaries (e.g., Working Group on California Earthquake Probabilities, 1988, 1990, 2002; *Nishenko* [1991]) although their validity has yet to be firmly established. Inherent in these models is the persistence of the distribution of strong and weak portions of the fault zone for consecutive large earthquakes and throughout the interseismic cycle. The implication is that weak regions slip relatively freely at or near the plate rate (generating abundant small earthquakes), loading the adjacent strong regions (that are completely locked) until failure occurs in a large earthquake. This concept has been used to identify asperities of future earthquakes from gaps in microseismicity patterns. For northeastern Japan, *Igarashi et al.* [2003] found that frequently repeating small earthquakes and adjacent freely slipping regions co-locate with low slip regions of coseismic moment release associated with two large plate boundary earthquakes in 1968 (Mw =8.2) and 1994 (Mw=7.7). Their distribution of “aseismic”

slip (or “microseismic” slip) obtained from the repeating earthquakes also matches the pattern of freely slipping regions estimated from GPS. *Zweck et al.* [2002] document persistence of large asperities in the Alaska-Aleutian suduction zone, noting a correspondence between regions of interseismic strain accumulation and patches of high coseismic slip for the great 1964 (Mw=9.2) Alaskan earthquake. These observations are consistent with a simple characteristic earthquake model, and persistence of locking patterns through more than one seismic cycle.

However, studies of other subduction zones have suggested that the location of strong and weak regions could vary between consecutive great earthquakes. For example, *Schwartz* [1999] compared the spatial distribution of moment release for consecutive earthquake ruptures along four different subduction zones and found non-characteristic behavior. While two of the earthquake pairs re-ruptured portions of the same asperity distribution, the other two events filled in areas of slip deficit left by preceding events. *Hirose and Hirahara* [2002] performed numerical simulations with realistic friction conditions and suggested that asperities with large dimensions along strike tend to only partially rupture in a given earthquake, so that long term behavior may be complex. The Nicoya region may also exhibit complex behavior, even though the asperities here are relatively small. While the up-dip and down-dip limits are similar, the rupture area of the 1978 earthquake is less than half the area of the 1950 event, i.e., along strike rupture length can be highly variable.

Bilek et al. [2003] related earthquake rupture complexity along the Costa Rican subduction zone to morphologic features on the subducting plate. For central Costa Rica, where incoming lithosphere is relatively rough, they suggested that seamounts or bathymetric highs subducted to seismogenic depths act as regions of enhanced locking. These regions should persist over many seismic cycles. However, in the Nicoya region, where incoming lithosphere is relatively smooth, the locked patches are elongated parallel to the trench, orthogonal to the orientation of seamount chains on the visible portion of the Cocos plate. Perhaps if subducting lithosphere is relatively smooth, temperature-controlled metamorphic phase changes and resulting changes in pore fluid pressure in the sediment column control the location of locking.

Additional evidence that locked portions of the plate interface may persist beyond a single earthquake cycle comes from extending the characteristic earthquake model to very small magnitude events. Small repeating earthquake clusters in continental strike-slip zones [*Nadeau et al.* 1995; *Nadeau and McEvilly*, 1999; *Burgman et al.*, 2000] have been interpreted as repeated failure of small asperities (with dimensions from 10-1000 m) driven by stable sliding of the intervening regions (the small events may be considered to have recurrence intervals of weeks to months). This has allowed determination of the spatio-temporal distribution of aseismic slip from the recurrence interval and estimated slip in the repeating earthquakes, and confirmed the essential aspects of a simple characteristic earthquake model for small events, at least over several seismic cycles.

7.3 Locked vs Creeping Sections and Partial Coupling of the Seismogenic Zone

The relation of microseismicity to locked and slipping patches observed in Nicoya has also been noted in continental strike slip faults. *Nadeau and Johnson* [1998] compared the locations of repeating microearthquakes with locked and creeping patches on the Parkfield section of the San Andreas fault based on geodetic studies by *Harris and Segall* [1987]. They also found repeating microearthquakes concentrated in the creeping section. *Malservisi* [2002] reports concentrations of microearthquakes at transition zones between locked and more freely slipping regions of the Hayward Fault in California, interpreted to indicate accelerated strain accumulation at the transitions. Increased strain at locked to creeping transition zones could deform the surrounding volume and hence might explain the abundant upper plate as well as interplate seismicity near the strongest gradient in locking (Figure 16).

Many subduction zones have been determined to be “partially coupled” based on a comparison between seismic moment release rates and the full plate convergence rate [e.g., *Pacheco et al*., 1993]. *McCaffrey* [1997] and *Norabuena et al.* [1998] discuss the difficulties inherent in these estimates. Partial coupling has also been reported in geodetic studies. While we can generate a uniform slip solution in Nicoya with a partially locked seismogenic zone (approximately 35-40% of the plate rate), the data density here allows much finer resolution, and indicates that the seismogenic plate interface here is better represented by relatively small fully locked (or nearly so) patches,

surrounded by regions that are essentially freely slipping. This suggests that some subduction thrusts, previously inferred to be partially coupled based on seismic data or spatially limited geodetic data, might be better represented by alternating locked and slipping regions; the degree of coupling would therefore represent the relative areas of these two contrasting types of mechanical behavior. Spatially dense geodetic data are required to investigate this issue.

7.4 Seismic Hazard.

The Osa region experienced a M_w 7.4-7.5 underthrusting earthquake in 1983 [*Adamek et al.*, 1988; *Tajima and Kikuchi*, 1995) as well as similar size events in 1904 (Mw=7.2), and 1941 (M_w=7.4) [*Protti et al.*, 1994]. Other than location and approximate magnitude, characteristics of the 1904 event are not well known [*Pacheco and Sykes*, 1992]. *Adamek et al*. [1988] conclude that the 1941 and 1983 events were similar, and computed rupture dimensions and mean slip for the 1983 event of 70 km by 110 km ($7.7x10^3$ km^2) and 0.58 m respectively. *Tajima and Kikuchi* [1995] re-studied this event and suggested that the rupture area was overestimated in the original study, while the mean slip was underestimated. *Tajima and Kikuchi* [1995] also found that the 1983 event includes a strike slip sub-event to the southeast. Given the largest seismic moment reported for this event (1.8×10^{20} N-m, from the Harvard Centroid Moment Tensor solution), the smaller rupture area (6.6×10^3 km^2) reported by *Tajima and Kikuchi* [1995], and shear modulus $3x10^{10}$ N/m^2, the maximum slip in the 1983 event is about 0.9 m.

Our analysis suggests that the plate boundary here is fully locked at present. If the rate of strain accumulation is constant, we can estimate the approximate time until the next (1983-like) event, assuming a simple characteristic earthquake model. Assuming total slip in 1983 was 0.9 m, that the accumulation rate is 6 cm/yr, and that all strain releases seismically, the recurrence interval is 17 years, shorter than the nominal 40 year interval noted above. This implies that either the strain accumulation rate is not constant, the elastic strain on the plate boundary is smaller than our estimate (e.g., additional slip in the Fila Costena) or that total slip in 1983-like events (including afterslip) is larger than 0.9 meters (2.4 meters of slip and 6 cm/yr of elastic accumulation give a 40 year recurrence interval). In terms of seismic hazard, earthquakes should also occur in the Fila

Costena and back arc regions. While strain accumulates more slowly in these regions, suggesting less frequent events, such events could actually be more damaging because their epicenters may be closer to populated regions.

From a seismic hazard perspective, perhaps the most important general result from our Nicoya observations is that we may be able to place constraints on the size of the next major earthquake from geodetic observations during the interseismic phase, since interseismic locked zones presumably rupture in the next major earthquake. The locked patches that we infer from our inversion include areas last ruptured in 1950 (Mw=7.7) and 1978 (Mw=7.0). The 1990 event (Figure 17) mostly ruptured to the south, and hence did not release significant strain in the Nicoya area [*Protti et al*., 1995]. Most of the rupture area of the 1950 event apparently is not currently accumulating strain at a high rate, and may even be freely slipping (Figure 17). The 1978 event ruptured only a small portion of the up-dip geodetically locked patch (relocated aftershock area in Figure 17) and released approximately 0.6 m of accumulated strain [*Guendel*, 1986]. Thus, most areas that we infer to be locked and accumulating strain have not had a significant earthquake in 53 years, representing a seismic gap that may be the locus of a future event. The size of such an event depends on the rupture area. Using empirical scaling relations for rupture area and moment magnitude [*Wells and Coppersmith*, 1994], if only a relatively small patch on the plate interface ruptures (e.g., the shallow one centered at 14 km depth), the resulting earthquake would be relatively small, perhaps M~7.0. However, if both the up and down-dip locked patches rupture, the future event could be comparable to the larger 1950 event.

7.4 Longer Time Scale Deformation

7.4.1 Trench-Parallel Fore Arc Block Motion. We estimate trench-parallel motion of the Nicoya fore-arc to the northwest at a rate of 8±3 mm/yr. *McCaffrey* [2002] inverted the data of *Lundgren et al.* [1999] for strain accumulation of the plate interface and rigid-body rotation of the fore-arc block assuming spherical geometry, obtaining 5±6 mm/yr of fore arc block motion (our estimate assumes simple Cartesian geometry, ignoring earth curvature which is small over the region of interest, but accounts for post-seismic

response to the 1992 Nicaragua earthquake). These two geodetic estimates are equivalent within uncertainties; both are slower than the 14±2 mm/yr of block translation estimated by *DeMets* [2001] for the Nicaraguan fore-arc based on earthquake slip vector azimuths. Some of the difference may reflect the fact that both geodetic estimates in Costa Rica treat the Nicoya fore-arc as a single block, whereas it is possible that only the northern portion of the block translates at the higher rate inferred for Nicaragua. The geometry of the trench is such that oblique convergence is only defined for roughly the northern half of the Nicoya peninsula (Figure 1). For the southern half, convergence is essentially trench-normal. The geodetic estimates of Nicoya block translation rate (5-8 mm/yr) may therefore reflect an average between ~14 mm/yr to the north and essentially zero to the south. Higher spatial sampling of the surface velocity field as well as more sophisticated modeling will be required to verify this and to define the region where northwest translation begins.

The structures that might accommodate northwest block motion are not clear. Northwest-striking right-lateral strike-slip faults are not well developed in northern Costa Rica, but could be obscured by recent volcanic deposits. Diffuse right-lateral shear could be accommodated within the thermally weak volcanic arc or the nearby Tempisque Basin (Figure 1). Block translation could also occur by vertical axis rotation of smaller blocks defined by short, northeast striking, left-lateral "bookshelf" faults, as observed in Nicaragua [*LaFemina et al.,* 2002]. Our GPS data are not adequate to distinguish between these hypotheses. Focal mechanisms of smaller magnitude earthquakes recorded during our seismic deployment also do not show a clear pattern. However, several moderate magnitude historical earthquakes along the northern volcanic arc have damaged that region, in 1911 (between Arenal and Tenorio volcanoes), 1935 (Bagaces, southwest of Miravalles volcano), and 1973 (Tilaran, m_b=5.7, right lateral strike slip on a northwest striking fault [*Guendel,* 1986]). Beginning in August-October 2003 a seismic swarm occurred around Tenorio volcano. The largest event was M~3.8, associated with right lateral strike slip on a northwest striking fault (Waldo Taylor, written com.).

7.4.2. Crustal shortening and mountain building.

The ~7 cm/yr of locked slip on the main plate boundary that we infer for the Osa segment is twice as high as the Nicoya segment (3.6 cm/yr; Table 5). Assuming these patterns are correct and extend over multiple seismic cycles, then this contrast in short term mechanical behavior of the plate interface may explain differences in longer term geologic processes (Table 5).

The development of the western portion of the North Panama fold and thrust belt is generally ascribed to subduction of the aseismic Cocos Ridge [*Plafker and Ward*, 1992; *Suarez et al.*, 1995; *Collins et al.*, 1995; *Silver et al.*, 1995; *Tajima and Kikuchi*, 1995; *de Boer et al.*, 1995; *Kolarsky et al.*, 1995]. Development of the Fila Costena may also relate to this event [*Protti et al.*, 1995; *Fisher et al*., 2003]. Both features are also probably influenced by the young (15-16 Ma) age of subducting lithosphere here.

We suggest that the different locking patterns in the Osa and Nicoya regions similarly reflect the combined influence of contrasting sea floor age and subduction of the shallow Cocos Ridge, in effect providing the mechanical link between long term geological processes and the character of subducted sea floor. Subduction of the shallow Cocos ridge mimics the effect of young lithosphere, subduction of which is often associated with a high degree of locking [*Ruff and Kanamori*, 1980]. The combined effect of young age and shallow bathymetry implies that subducted lithosphere beneath Osa is anomalously buoyant, promoting mechanical coupling over a large depth range.

Two other important differences between the regions are the presence of a volcanic arc and subduction obliquity in the north, and their absence in the south. Margin-parallel block transport in the north can be considered as a form of tectonic escape, insulating the back arc there from fore-arc compressive stresses, which are in any case small due to the relatively small area of locked patches on the plate interface. The presence of an active volcanic arc in the north may facilitate mechanical isolation of the back arc, representing a trench-parallel zone of weakness that can accommodate trench parallel fore arc motion. In the south, orthogonal convergence, lack of a volcanic arc, and lack of a tectonic escape mechanism means that the high compressive stresses associated with short term elastic deformation and a fully locked plate boundary can be transmitted through the rigid upper plate, promoting permanent crustal shortening in the upper plate wherever these stresses exceed some threshold for brittle failure.

Constraints on Timing. Have differences in mechanical coupling between the two regions persisted long enough to influence geological development? If our hypothesis linking coupling with differences in seafloor age and subduction of the Cocos ridge is correct, this can be addressed in several ways. The relative age difference for subducted seafloor between Nicoya and Osa has persisted for at least the last few million years, based on analysis of magnetic lineations and plate reconstruction [*Barckhausen et al*., 2001]. The Cocos Ridge began subducting sometime after 6 Ma, although there is uncertainty in the exact timing. *DeBoer et al.* [1995] suggest initiation at about 5 Ma based on changes in arc magmatism. *Lonsdale and Klitgord* [1978] suggest initiation at about 1 Ma based on magnetic anomaly patterns on the Cocos plate. *Collins et al.* [1995] prefer an age of 3.6 Ma based on a detailed uplift history for the region from paleobathymetries of dated stratigraphic sections. Assuming 2 cm/yr of long term shortening (1.0 cm/yr in both the fore-arc and back arc, based on the GPS data) for the last 3 million years gives 60 km of total shortening. *Fisher et al.* [2003] document a minimum of 17.4 km of shortening in the Fila Costena during the last 2 Ma. This process may have contributed to contrasts in crustal thickness and mean elevation of the two regions (Figure 16).

8. CONCLUSIONS

1. The up-dip limit of the seismogenic zone in the Nicoya peninsula of Costa Rica, as determined from geodetic measurements of strain accumulation, differs significantly from interseismic microseismicity recorded during 1999-2000. Geodetically determined locking based on GPS observations between 1994 and 2000 begins at ~8 km depth and peaks at ~14 km depth. This is well up-dip of microseismicity but is close to the up-dip rupture limit of past large earthquakes.

2. The geodetically determined up-dip limit of the seismogenic zone corresponds approximately with the 100°C isotherm. Both of these entities shallow across the change in oceanic crustal origin from the East Pacific Rise to the Cocos-Nazca spreading center.

3. Locked portions of the plate interface in the Nicoya area do not experience significant microseismicity during the interseismic part of the earthquake cycle; more freely slipping regions do experience microseismicity. If this pattern persists through the

entire interseismic part of the cycle, then the locked portions can be expected to contribute significant moment (i.e., rupture with large slip) in the next major earthquake, while the microseismic regions would presumably rupture by smaller amounts and contribute less moment.

4. The Nicoya fore-arc block translates northwest at an average rate of 8±3 mm/yr.

5. Relative plate motion in the Osa region of Costa Rica is partitioned between the Pacific (Cocos-Panama block) boundary, accommodating ~8 cm/yr (~1 cm/yr of this probably represents permanent shortening across the Fila Costena fold and thrust belt, while the remainder represents elastic strain accumulation on the main plate boundary), and the Caribbean (Panama block-Caribbean plate) boundary, accommodating ~1 cm/yr shortening across the North Panama fold and thrust belt.

Acknowledgments. We thank NSF's MARGINS program (grants OCE 99 05469 to THD; OCE9910609 to SYS; and OCE9910350 to LMD) and Germany's BMBF (grant 03G0144) and SFB 574 of Christian Albrechts University of Kiel for providing funds for these joint marine and on-land observations. We thank personnel of the F/S Sonne and R/V Melville for deployment and recovery of the OBS and OBH. Some of the land seismic instrumentation was provided by the PASSCAL facility of the Incorporated Research Institutions for Seismology (IRIS) through the PASSCAL instrument center at New Mexico Tech. Data from these stations is available through the IRIS Data Management Center. Many of the GPS receivers, and technical assistance for their deployment, were provided by UNAVCO. The GPS data are available at the UNAVCO archive. We also thank personnel at OVSICORI-UNA, including E. Hernandez, R. van der Laat and Tomas Marino for their assistance in GPS and seismic data collection. Reviews by Seth Stein, Stephane Mazzotte, and Jeff Freymueller significantly improved the manuscript.

References

Adamek, S., F. Tajima, D. Wiens, Seismic rupture associated with subduction of the Cocos Ridge, Tectonics, 6, 757-774, 1987.

Avants, M., S. Schwartz, A. Newman, H. DeShon, Large underthrusting earthquakes beneath the Nicoya Peninsula, EOS: Trans. Am. Geophys. U., 82, F1266, 2001.

Barckhausen, U., C. R. Ranero, R. von Huene, S. C. Cande, H. A. Roeser, Revised tectonic boundaries in the Cocos Plate off Costa Rica: Implications for the segmentation of the convergent margin and for plate tectonic models, *J. Geophys. Res., 106*, no.B9, p. 19,207-19220, 2001.

Beck, M.E., Jr., Coastwise transport reconsidered: lateral displacements in oblique subduction zones, and tectonic consequences, *Phys. Earth Plan. Inter., 68*, 1-8, 1991.

Bialas, J., E.R. Flueh, G. Bohrmann, (Eds), FS Sonne cruise report SO144/1&2: PAGANINI, GEOMAR Report 102, Kiel, Germany, 437pp, 1999.

Bilek, S.L., S.Y. Schwartz, and H.R. DeShon, Control of seafloor roughness on earthquake rupture behavior, *Geology, 31*, 455-458, 2003.

Boucher, C., Z. Altamimi, P. Sillard, The 1997 International Terrestrial Reference Frame (ITRF-97), *IERS Tech. Note, 27*, Obs. de Paris, Paris, 1999.

Bürgmann, R. D. Schmidt, R.M. Nadeau, M. d'Alessio, E. Fielding, D. Manaker, T.V. McEvilly, and M.H. Murray, Earthquake potential along the northern Hayward fault, California, *Science*, 289, 1178-1181, 2000.

Bürgmann, R., M. G. Kogan, V. E. Levin, C. H. Scholz, R. W. King, G. M. Steblov, Rapid aseismic moment release following the 5 December 1997 Kronotsky Kamchatka earthquake, *Geophys. Res. Letters, 28*, 1331-1334, 2001.

Byrne, D. E., D. Davis, and L. Sykes, Loci and maximum size of thrust earthquakes and the mechanics of the shallow region of subduction zones, *Tectonics, 7*, 833-857, 1988.

Case, J. E., T. L. Holcombe, Geologic map of the Caribbean region, U.S. Geological Survey, Miscellaneous Investigations Map, I-1100 (Scale 1: 2,500,000), 1980.

Christensen, Douglas H. and Ruff, Larry J., Seismic Coupling and Outer Rise Earthquakes, *J. Geophys. Res., 93*, 13,421-13,444, 1988.

Christeson, G. L., K. D. McIntosh, T. H. Shipley, E. R. Flueh, and H. Goedde, Structure of the Costa Rica convergent margin, offshore Nicoya Peninsula; *J. Geophys. Res., 104*, 11, 25443-25468, 1999.

Collins, L. S., A. Coates, J. Jackson, J. Obando, Timing and rates of emergence of the Limon and Bocas del Toro basins: Caribbean effects of Cocos Ridge subduction? in P. Mann, ed., Geologic and tectonic development of the Caribbean plate boundary in South America, *GSA Special Paper 295*, 263-290, 1995.

Corrigan, J., P. Mann, J. Ingle, Forearc response to subduction of the Cocos Ridge, *Geol. Soc. Am. Bull., 102*, 628-652, 1990.

De Boer, J. Z., M. S. Drummond, M. J. Bordelon, M. J. Defant, H. Bellon, R. C. Maury, Cenozoic magmatic phases of the Costa Rican island arc (Cordillera de Talamanca), in P. Mann, ed., Geologic and tectonic development of the Caribbean plate boundary in South America, *GSA Special Paper 295*, 35-55, 1995.

DeMets, C., R. G. Gordon, D. F. Argus, and S. Stein, Effect of recent revisions to the geomagnetic time scale on estimates of current plate motion, *Geophys. Res. Lett., 21*, 2191-2194, 1994.

DeMets, C., A new estimate for Cocos-Caribbean plate motion: implications for slip along the Central American volcanic arc, *Geophys. Res. Lett., 28*, 4043-4046, 2001.

DeShon, H.R. S.Y. Schwartz, S.L. Bilek, L.M. Dorman, V. Gonzalez, J.M. Protti, T. H. Dixon, and E.R. Flueh, Seismogenic zone structure of the southern middle America Trench, Costa Rica, *J. Geophys. Res*., 108,doi 10.1029/2002JB002294, 2003a.

DeShon, H., S. Schwartz, A. Newman, L. Dorman, M. Protti, L. Gonzalez, Geometry and velocity structure of the northern Costa Rica seismogenic zone from 3-D local earthquake tomography, EOS: Trans. Am. Geophys. U., 84 (6), F1420, Fall Mtg Supp., 2003b.

Dixon, T. H. GPS measurements of relative motion of the Cocos and Caribbean plates and strain accumulation across the Middle America Trench, *Geophys. Res. Lett., 20*, 2167-2170, 1993.

Dixon, T. H. and S. Kornreich Wolf, Some tests of wet tropospheric calibration for the Casa Uno GPS experiment, *Geophys. Res. Lett., 17*, 203-206, 1990.

Dixon, T. H., M. Miller, F. Farina, H. Wang, D. Johnson, Present-day motion of the Sierra Nevada block and some tectonic implications for theBasin and Range province, North American Cordillera, *Tectonics, 19*, 1-24, 2000.

Dixon, T. H., J. Decaix, F. Farina, K. Furlong, R. Malservisi, R. Bennett, F. Suarez Vidal, J. Fletcher, J. Lee, Seismic cycle and rheological effects on estimation of present-day slip rates for the Agua Blanca and San Miguel-Vallecitos faults, northern Baja California, Mexico, *J. Geophys. Res., 107*, B10, doi 10.1029/2000JB000099, 2002.

Fisher, A.T., C. A. Stein, R. N. Harris, K. Wang, E. A. Silver, M. Pfender, M. Hutnak, A. Cherkaoui, R. Bodzin, and H. Villinger, Abrupt thermal transition reveals hydrothermal boundary and role of seamounts within Cocos Plate; *Geophys. Res. Let*., 30, 11, 10.1029/2002GL016766, 2003.

Fisher, D. M., T. W. Gardner, P. B. Sak, Active thrusting in the inner fore-arc of an erosive convergent margin, Pacific coast, Costa Rica, (Tectonics, In Press, 2004).

Fitch, T.J., 1972, Plate convergence, transcurrent faults, and internal deformation adjacent to Southeast Asia and western Pacific, *J. Geophys. Res., 77*, no. 23, p. 4432-4460, 1972.

Gardner, T. W., D. Verdonck, N. Pinter, R. Slingerland, K. Furlong, T. F. Bullard, S. G. Wells, Quaternary uplift astride the aseismic Cocos Ridge, Pacific coast of Costa Rica, *Geol. Soc. Am. Bull., 104*, 219-232, 1992.

Goes, S. D. B., A. A. Velasco, S. Y. Schwartz, T. Lay, The April 22, 1991 Valle de la Estrella, Costa Rica (Mw=7.7) earthquake and its tectonic implications: a broadband seismic study, *J. Geophys. Res., 98*, 8127-8142, 1993.

Guendel, F. Seismotectonics of Costa Rica: an analytical view of the southern terminus of the Middle America Trench, PhD thesis, University of California, Santa Cruz, 1986.

Harris, R. N., and P. Segall, Detection of a locked zone at depth on the Parkefield, California segment of the San Andreas fault, *J. Geophys. Res., 92*, 7945-7962, 1987.

Harris, R. N., and K. Wang, Thermal models of the Middle America trench at the Nicoya Peninsula, Costa Rica, *Geophys. Res. Letters, 29*, 10.1029/2002GL015406, 2002.

Hey, R. N., Tectonic evolution of the Cocos-Nazca spreading center, *Geol. Soc. Am. Bull., 88*, 1404-1420, 1977.

Hirth, G., and D. L Kohlstedt, Water in the oceanic upper mantle: implications for rheology, melt extraction and the evolution of the lithosphere, *Earth Planet. Sci. Letters, 144*, 93-108, 1996.

Hitoshi, H., and K. Hirahara, A model for complex slip behavior on a large asperity at subduction zones, *Geophys. Res. Lett., 29*, 22, 2068, doi 10.1029/2002GL015825, 2002.

Husen, S., E. Kissling, E. Flueh, and G. Asch, Accurate hypocenter determination in the seismogenic zone of the subducting Nazca Plate in northern Chile using a combined on-/offshore network, *Geophys. J. Int., 138*, 687-701, 1999.

Hyndman, R. D. and K. Wang, Thermal constraints on the zone of major thrust earthquake failure: the Cascadia subduction zone, *J. Geophys. Res. 98*, 2039-2060, 1993.

Hyndman, R. D., K. Wang, and M. Yamano, Thermal constraints on the seismogenic portion of the southwest Japan subduction thrust, *J. Geophys. Res., 100*, 15,373-15,392, 1995.

Hyndman, R. D. and K. Wang, The rupture zone of Cascadia great earthquakes from current deformation and the thermal regime, *J. Geophys. Res. 100*, 22,133-22154, 1995.

Ide, S., F. Imamura, Y. Yoshida, K. Abe, Source characteristics of the Nicaragua tsunami earthquake of September 2, 1992, *Geophys. Res. Lett. 20,* 863-866, 1993.

Imamura, F., N. Shuto, S. Ide, Y. Yoshida, K. Abe, Estimate of the tsunam,I source of the 1992 Nicaragua earthquake from tsunami data, *Geophys. Res. Lett. 20,* 1515-1518, 1993.

Ihmle´, P. F., Frequency-dependent relocation of the 1992 Nicaragua slow earthquake: an empirical Green's function approach, *Geophys. J. Int., 127,* 75-85, 1996.

Igarashi, T., T. Matsuzawa, and A. Hasegawa, 2003. Repeating earthquakes and interplate aseismic slip in the northeastern Japan subduction zone, *J. Geophys. Res*. 108, 2249,doi.:10.1029/2002JB001920.

Jacobson, R. S., L. M. Dorman, M. Purdy, A. Schultz, S. C. Solomon, Ocean Bottom Seismometer facilities available, *EOS, Trans. Am. Geophys. Union, 72*(46), 405-515, 1991.

James, T. S., J. J. Clague, K. Wang, I. Hutchinson, Post-glacial rebound at the northern Cascadia subduction zone, *Quaternary Science Rev., 19,* 1527-1541, 2000.

Jarrard, R. D., Relations among subduction parameters, *Rev. Geophys., 24,* no. 2, p.217-284, 1986.

Kanamori, H., Mechanism of tsunami earthquakes, *Phys. Earth Planet. Int., 6,* 246-259, 1972.

Kanamori, H., and M. Kikuchi, The 1992 Nicaragua earthquake: a slow tsunami earthquake associated with subducted sediment, *Nature, 361,* 714-715, 1993.

Kikuchi, M., and H. Kanamori, Source characteristics of the 1992 Nicaragua tsunami earthquake inferred from teleseismic body waves, *Pure App. Geophys., 144,* 441-453, 1995.

Kohlstedt, D. L., B. Evans, and S. J. Mackwell, Strength of the lithosphere: constraints imposed by laboratory experiments, *J. Geophys. Res., 100,* 17,587-17,602, 1995.

Kolarsky, R. A., P. Mann, W. Montero, Island arc response to shallow subduction of the Cocos Ridge, Costa Rica, in P. Mann, ed., Geologic and tectonic development of the Caribbean plate boundary in South America, *GSA Special Paper 295,* 235-262, 1995.

LaFemina, P. C., T. H. Dixon, W. Strauch, Bookshelf faulting in Nicaragua, *Geology, 30,* 751-754, 2002.

Langseth, M. G., and E. A. Silver, The Nicoya convergent margin-a region of exceptionally low heat flow, *Geophys. Res. Letters, 23,* 891-894, 1996.

Linde, A. T., M. Gladwin, M. Johnston, R. Gwyther, R. Bilham, A slow earthquake sequence on the San Andreas fault, *Nature, 383*, 65-68, 1996.

Lonsdale, P. and Klitgord, K. D., Structure an tectonic history of the eastern Panama Basin, *Geol. Soc. Am. Bull., 89*, 981-999, 1978.

Lundgren, P., S. Wolf, M. Protti, K. Hurst, GPS measurements of crustal deformation following the 22 April 1991 Valle de Estrella Costa Rica earthquake, *Geophys. Res. Lett., 20*, 407-410, 1993.

Lundgren, P. M. Protti, A. Donnellan M. Heflin, E. Hernandez, D. Jefferson, Seismic cycle and plate margin deformation in Costa Rica: GPS observations from 1994 to 1997, *J. Geophys. Res., 104*, 28,915-28,928, 1999.

Malservisi, R., Numerical models of the dynamics of lithospheric deformation at complex plate boundaries, Ph.D. thesis, Pennsylvania State University, 120p., 2002.

Mao, A., G. G. H. Harrison, T. Dixon, Noise in GPS coordinate time series, *J. Jeophys. Res., 104*, 2797-2816, 1999.

Marshall, J. S., D. M. Fisher, T. W. Gardner, Central Costa Rica deformed belt: kinematics of diffuse faulting across the western Panama block, *Tectonics, 19*, 468-492, 2000.

McCaffrey, R., Oblique plate convergence, slip vectors, and forearc deformation, *J. Geophys. Res., 97*, 8905-8915, 1992.

McCaffrey, R., Statistical significance of the seismic coupling coefficient, *Bull. Seismol. Soc. Am., 87*, 1069, 1997.

McCaffrey, R., Crustal block rotations and plate coupling, in: Plate Boundary Zones, S. Stein and J. Freymueller, eds., *AGU Geodynamics Series, 20*, 101-122, 2002.

Murdoch, J. N., Comment on Discussions of ODP Leg 205 and drilling of Middle America seismogenic zone, *EOS: Trans. Am. Geophys. U., 84*, 303, 2003.

Nadeau, R. M., and L. R. Johnson, Seismological studies at Parkfield, VI: moment releas rates and estimates of source parameters for small repeating earthquakes, *Bull. Seismol. Soc. Am., 88*, 790-814, 1988.

Nadeau, R. M., W. Foxhall, T. V. McEvilly, Clustering and periodic recurrence of microearthquakes on the San Andreas fault at Parkfield, California, *Science, 267*, 503-507, 1995.

Nadeau, R.M. and T.V. McEvilly, Fault slip rates at depth from recurrence intervals of repeating microearthquakes, *Science,* 285, 718-721, 1999.

Newman, A.V., S. Schwartz, V. Gonzalez, H. DeShon, J. Protti, L. M. Dorman, Along-strike variability in the seismogenic zone below the Nicoya Peninsula, Costa Rica, *Geophys. Res. Lett., 29,* doi10.1029/2002GLO15402, 2002.

Nicol, A. amd J. Beavan, Shortening of an overriding plate and its implications for slip on a subduction thrust, central Hikurangi margin, New Zealand, Tectonics, 22, 1070, 10.1029/2003TC001521, 2003.

Norabuena, E., L. Leffler, A. Mao, T. Dixon, S. Stein, S. Sacks, M. Ellis, Space geodetic observation of Nazca-South America convergence along the central Andes, *Science, 279,* 358-362, 1998.

Obana, K., S. Kodaira, Y. Kaneda, K. Mochizuki, M. Shinohara, K. Suyehiro, Microseismicity at the seaward updip limit of the western Nankai Trough seismogenic zone, *J. Geophys. Res., 108*, B10, 1459, 10.1029/2002JB002370, 2003.

Oleskevich, D. A., R. D. Hyndman, K. Wang, The updip and downdip limits to great subduction earthquakes: thermal and struictural models of Cascadia, south Alaska, SW Japan and Chile, *J. Geophys. Res., 104*, 14,965-14,991, 1999.

Pacheco, J. F., L. Sykes, Seismic moment catalog for large shallow earthquakes from 1900 to 1989, *Bull. Seismol. Soc., 82*, 1306-1349, 1992.

Pacheco, J. F., L. Sykes, C. Scholz, Nature of seismic coupling along simple plate boundaries of the subduction type, *J. Geophys. Res., 98*, 14133-14,159, 1993.

Peacock, S., Large-scale hydration of the lithosphere above subducting slabs, *Chem. Geol., 108*, 49-59, 1993.

Peltier, W. R., Post-glacial variations in the level of the sea: implications for climate dynamics and solid earth geophysics, *Rev. Geophys., 36*, 603-689, 1998.

Plafker, G. and S. N. Ward, Thrust faulting and tectonic uplift along the April 22, 1991 Costa Rico earthquake, *Tectonics, 11*, 709-718, 1992.

Pollitz, F. F., Gravitational visco-elastic postseismic relaxation on a layered spherical Earth, *J. Geophys. Res., 102,* 17,921-17,941, 1997.

Pollitz, F. F., R. Burgmann, P. Segall, Joint estimation of afterslip rate and post-seismic relaxation following the 1989 Loma Prieta earthquake, *J. Geophys. R., 103*, 26,975-26,992, 1998.

Pollitz, F. F., G. Peltzer, R. Bürgmann, Mobility of continental mantle: evidence from post-seismic geodetic observation following the 1992 Landers earthquake, *J. Geophys. Res., 105*, 8035-8054, 2000.

Protti, M. and S. Schwartz, Mechanics of back arc deformation in Costa Rica, *Tectonics, 13*, 1093-1107, 1994.

Protti, M., F. Guendel, and K. McNally, Geometry of the Wadati-Benioff zone under South America and its tectonic significance, *Phys. Earth Plan. Int., 84*, 271-287, 1994.

Protti, M., and 14 others, The March 25, 1990 (Mw = 7.0, ML = 6.8), earthquake at the entrance of the Nicoya Gulf, Costa Rica; its prior activity, foreshocks, aftershocks, and triggered seismicity, *J. Geophys. Res., 100,* 10, 20,345-20,358, 1995a.

Protti, M., F. Guendel, and K. McNally, Correlation between the age of the subducting Cocos plate and the geometry of the Wadati-Benioff zone under Nicaragua and Costa Rica, in Geologic and Tectonic Development of the Caribbean Plate Boundary in Southern Central America, Special Paper 295, ed. P. Mann, GSA, Boulder, CO, 309-326, 1995b.

Protti, M., S.Y. Schwartz, and G. Zandt, Simultaneous inversion for earthquake location and velocity structure beneath Costa Rica, *Bull. Seismol. Soc. Am., 86*, 19-31, 1996.

Protti, M. Güendel, F. and Malavassi, E., Evaluación del Potencial Sísmico de la Península de Nicoya; Editorial Fundación UNA, 1st. edition, Heredia, Costa Rica, 144 p., 2001.

Ranero, C.R., and R. von Huene, 2000. Subduction erosion along the Middle America convergent margin, *Nature, 404*, 748-752.

Ruff, L. and H. Kanamori, Seismicity and the subduction process, *Phys. Earth Planet. Int., 23*, 240-252, 1980.

Ruff, L. and H. Kanamori, H., Seismic coupling and uncoupling at subduction zones, *Tectonophysics, 99*, 99-117, 1983.

Ruff, L., Asperity distributions and large earthquake occurance in subduction zones, *Tectonophysics, 211*, 61-83, 1992.

Sallarès, V., J. J. Dañobeitia, E. R. Flueh, and G. Leandro, Seismic velocity structure across the Middle American landbridge in Northern Costa Rica; *J. Geodynamics, 27*, 327-344, 1999.

Sallarès, V., J. J. Dañobeitia, and E. R. Flueh, Seismic tomography with local earthquakes in Costa Rica, *Tectonophysics, 329*, 61-78, 2000.

Sallarès, V., J. J. Dañobeitia, and E. R. Flueh, Lithospheric structure of the Costa Rica Isthmus: Effects of subduction zone magmatism on an oceanic plateau, *J. Geophys. Res., 106*, 621-643, 2001.

Satake, K., Mechanism for the 1992 tsunami earthquake, *Geophys. Res. Lett., 21*, 2519-2522, 1994a.

Satake, K., Mechanism of the 1992 Nicaragua "tsunami" earthquake, *Seism. Res. Lett., 65*, 1, 24, 1994b.

Satake, K., Linear and nonlinear computations of the 1992 Nicaragua earthquake tsunami, *Pure and Appl. Geophys., 144*, 455-470, 1995.

Satake, K. and Y. Tanioka, Source of tsunami and tsunamigenic earthquakes in subduction zones, in: Seismogenic and tsunamigenic processes in shallow subduction zones, J. Sauber and R. Dmovska, eds., *Pageoph., 154*, 467-484, 1999.

Sauter, A.W. and L. M. Dorman, A Deep-Water Seafloor Implosive Source with Applications for Off-Shore Instrumented Oil Fields and Sub-Sea Exploration, AAPG Annual Meeting, Houston, 2002.

Sauter, A. W., J. Hallinan, R. Currier, T. Barash, B. Wooding, A. Schultz, L. M. Dorman, A new ocean bottom seismometer, Proc. Conf. Marine Instrumentation '90, MPL-U-125/90, Marine Technology Society, 99-104, 1990.

Savage, J. C., A dislocation model of strain accumulation and release at a subduction zone, *J. Geophys. Res., 88*, 4984-4996, 1983.

Schwartz, S.Y., Source parameters of aftershocks of the 1991 Costa Rica and 1992 Cape Mendocino, California earthquakes from inversion of local amplitude ratios and broadband waveforms, *Bull. Seismol. Soc. Am., 85*, 1560-1575, 1995.

Schwartz, S. Y., Non-characteristic behavior and complex recurrence of large subduction zone earthquakes, *J. Geophys. Res., 104*, 23,111-23,125, 1999.

Schwartz, S.Y., A.V. Newman, M. Protti, and M. Vallee, A large tensional outer-rise earthquake in the Nicoya seismic gap, Costa Rica, *EOS Trans. AGU*, 82 (47), Fall Suppl., Abstract S12B-0600, 2001.

Sella, G., T. H. Dixon, and A. Mao, REVEL: A model for Recent plate velocity from space geodesy, *J. Geophys. Res., 107*, B4, 10.1029/2000JB000033, 2002.

Silver, E. A., D. L. Reed, J. E. Tagudin, D. J. Heil, Implications of the north and south Panama thrust belts for the origin of the Panama orocline, *Tectonics, 9*, 261-281, 1990.

Silver, E. A., J. Galewsky, K. D. McIntosh, Variation in structure, style and driving mechanism of adjoining segments of the North Panama deformed belt, in: P. Mann, ed., Geologic and Tectonic Development of the Caribbean Plate Boundary in Southern Central America, 225-234, *Geol. Soc. Am. Special Paper 295*, GSA, Boulder, Colorado, 349p., 1995.

Spinelli, G. A., and D. M. Saffer, Along-strike variations in underthrust sediment dewatering on the Nicoya margin, Costa Rica related to the updip limit of seismicity, *Geophys. Res. Lett., 31*, L04613, doi:10.1029/2003GL018863, 2004.

Stavenhagen, A. U., E. R. Flueh, C. Ranero, K. D. McIntish, T. Shipley, G. Leandro, A. Schulze, J. J. Danobeitia, Seismic wide angle investigations in Costa Rica, *Zbl. Geol. Palaont., Teil 1* (3-6), 393-408, 1997.

Suarez, G., M Pardo, J. Dominguez, L. Ponce, W. Montero, I. Boschini, W. Rojas, The Limon, Costa Rica earthquake of April 22, 1991: back arc thrusting and collisional tectonics in a subduction environment, *Tectonics, 14*, 518-530, 1995.

Tajima, F., and M. Kikuchi, Tectonic implications of the seismic ruptures associated with the 1983 and 1991 Costa Rica earthquakes, in: P. Mann, ed., Geologic and Tectonic Development of the Caribbean Plate Boundary in Southern Central America, 327-340, *Geol. Soc. Am. Special Paper 295*, GSA, Boulder, Colorado, 349p., 1995.

Tichelar, B. W. and L. Ruff, Depth of seismic coupling along subduction zones, *J. Geophys. Res., 98*, 2017-2037, 1993.

Tryon, M.D., K.M. Brown, A. Sauter, L. M. Dorman, A new benthic aqueous flux meter for very low to moderate discharge rates, *Deep Sea Res., 48*, I, 2121-2146, 2001.

Tryon, M.D., K.M. Brown, M. E. Torres, Fluid and chemicl fluxes in nd out of sediments hosting methane hydrate deposits on hydrate Ridge, Oregon, II: Hydrologic processes, *Earth Planet. Sci. Lett., 201*, 541-557, 2002.

Vergara-Munoz, A., Tectonic patterns of the Panama Block deduced from seismicity, gravitational data and earthquake mechanisms: implications to the seismic hazard, *Tectonophys. 154*, 253-267, 1988.

Von Huene, R., and 16 others, Morphotectonics of the Pacific convergent margin of Costa Rica, in: Geologic and Tectonic Development of the Caribbean Plate Boundary in Southern Central America, Special Paper 295, ed. P. Mann, GSA, Boulder, CO, 291-307, 1995.

Walther, C.H.E., E.R. Flueh, C.R. Ranero, R. von Huene, and W. Strauch, 2000. Crustal structure across the Pacific margin of Nicaragua: evidence for ophiolitic basement and a shallow mantle sliver, *Geophys. J. Int., 141*, 759-777.

Walther, C. and Flueh, E., 2002: Remnant of the ancient Farallon Plate breakup: A low-velocity body in the lower oceanic crust off Nicoya Peninsula, Costa Rica – evidence from wide-angle seismics; *Geophys. Res. Lett.*, 29(19), 1939, doi:10.1029/2002 GL015026.

Walther, C. H. E., 2003: The crustal structure of Cocos Ridge off Costa Rica; J. Geophys. Res., 108, 3, 2136, doi:10.1029/2001JB000888.

Weyl, R., 1980, Geology of Central America, p. 371, Gebruder Borntraeger, Berlin.

Ye, S., J. Bialas, E.R. Flueh, A. Stavenhagen, R. von Huene, G. Leandro, and K. Hinz, 1996. Crustal structure of the Middle American Trench off Costa Rica from wide-angle seismic data, *Tectonics, 15*, 1006-1021.

Zweck, C., Freymueller, J.T., and Cohen, S.C., 2002, Three-dimensional elastic dislocation modeling of the postseismic response to the 1964 Alaska earthquake, *J. Geophys. Res., 107*(B4), doi:10.1029/2001JB000409.

Table 1. GPS site velocities (mm/yr) relative to ITRF-97[1].

Station Name	Lat. ºN	Lon. ºW	Height m	Vn mm/yr	Ve mm/yr	Vv mm/yr
ACOS	10.54	84.60	300	07.5±1.2	17.0±1.5	2.5±3.1
AGUJ	09.72	84.62	71	14.5±1.0	15.8±2.7	-0.2±2.9
BALL	10.38	85.44	118	16.9±3.2	10.5±3.2	4.5±6.3
CABU	10.13	84.77	499	12.7±1.2	15.3±1.8	-1.6±3.6
CRUZ	11.05	85.63	267	11.4±1.7	05.8±2.5	-5.1±3.9
ETCG	09.99	84.10	1194	08.8±1.1	12.9±2.6	14.7±6.2
GRAN	10.56	85.65	122	15.6±1.6	9.3±1.7	0.0±3.1
GUAR	10.14	85.44	135	24.0±2.6	18.4±3.8	2.7±4.1
INDI	09.86	85.50	75	26.8±4.2	16.6±4.5	-10.2±7.1
JICA	09.97	85.13	61	15.7±1.6	15.6±2.9	-1.1±2.8
LIBE	10.65	85.42	223	16.7±2.1	12.6±3.4	0.9±6.5
MATA	10.35	85.81	78	15.7±1.3	9.9±2.1	0.6±3.3
PAQU	09.83	84.95	80	16.9±1.6	12.0±2.7	2.1±4.0
SAMA	09.88	85.54	46	28.1±1.5	17.4±1.9	-16.0±4.8
SJOS	10.36	84.94	1062	15.0±1.6	15.0±1.3	-4.4±4.7
SJUA	10.06	85.75	44	19.6±1.5	21.2±3.9	-4.7±3.2
ZUMA	09.65	85.08	214	10.3±3.3	8.3±4.1	-13.1±8.7
BRAT	09.55	82.89	60	13.8±1.0	17.9±3.7	-7.8±4.0
CAMP	08.63	82.83	927	16.5±2.4	23.0±1.2	-1.2±3.9
CARA	08.44	83.46	18	30.3±1.2	27.4±2.3	4.2±4.1
LIMO	09.96	83.03	13	5.0±2.1	17.5±3.3	-14.6±6.9
MANZ	09.61	82.67	185	9.9±4.1	22.1±6.8	-15.1±11.9
TIGR	09.04	83.29	696	31.3±4.2	33.9±9.3	-10.7±5.7
VUEL	09.62	83.85	3173	10.9±2.3	16.1±5.8	13.0±5.5

1. *Boucher et al.* [1999].

Table 2: Horizontal velocities relative to stable Caribbean Plate[1].

Station Name	Vn mm/yr	Ve mm/yr
ACOS	4.9±1.5	3.1±1.6
AGUJ	11.9±1.3	1.5±2.8
BALL	14.6±3.3	-3.5±3.3
CABU	10.2±1.5	1.2±1.9
CRUZ	9.2±1.9	-7.8±2.6
ETCG	6.0±1.4	-1.2±2.7
GRAN	13.4±1.8	-4.6±1.8
GUAR	21.8±2.8	4.3±3.9
INDI	24.6±4.3	2.4±4.5
JICA	13.3±1.8	1.5±3.0
LIBE	14.4±2.3	-1.2±3.5
MATA	13.6±1.6	-4.1±2.2
PAQU	14.4±1.8	-2.2±2.8
SAMA	25.9±1.8	3.2±2.0
SJOS	12.7±1.9	1.0±1.4
SJUA	17.5±1.8	7.1±3.9
ZUMA	7.9±3.4	-6.0±4.1
BRAT	10.5±1.3	3.5±3.8
CAMP	13.2±2.5	8.2±1.4
CARA	27.4±1.4	13.0±2.8
LIMO	1.7±1.2	3.3±2.2
MANZ	6.5±4.2	7.8±6.8
TIGR	28.2±4.3	19.3±9.3
VUEL	8.0±2.5	1.8±5.8

1. Caribbean plate definition based on GPS data in *Sella et al.* [2002].

Table 3. Data quantity and quality

SITE	Time span (years)	Number of Data (Days)	WRMS (mm)		
			N	E	V
ACOS	6.082	25	4.6	6.9	14.9
AGUJ	6.035	13	8.1	10.0	10.9
BALL	3.203	9	5.9	6.7	13.2
CABU	6.027	14	4.1	7.5	15.3
CRUZ	6.104	14	7.3	10.5	17.2
ETCG	6.254	26	4.6	12.9	33.5
GRAN	6.052	15	6.1	6.8	12.9
GUAR	3.208	10	4.3	8.6	8.3
INDI	2.816	19	8.8	10.1	16.2
JICA	6.049	17	5.3	12.0	11.8
LIBE	3.238	19	4.5	8.2	17.0
MATA	5.997	15	3.9	9.3	13.6
PAQU	6.019	16	5.2	11.7	18.0
SAMA	6.043	15	4.3	8.1	22.3
SJOS	6.038	12	6.2	5.6	20.8
SJUA	6.038	14	4.6	11.1	12.6
ZUMA	1.972	7	3.9	5.5	10.6
BRAT	6.098	11	3.7	14.2	16.5
CAMP	6.084	10	7.7	5.0	15.5
CARA	6.035	11	4.5	9.5	17.2
LIMO	2.035	9	2.7	4.8	8.5
MANZ	2.008	9	4.4	8.6	17.0
TIGR	2.005	7	4.3	11.7	5.7
VUEL	6.027	12	7.9	18.4	24.8

Table 4. Large Earthquakes Since 1980, Costa Rica and Nicaragua

Date	Lat. (ºN)	Lon. (ºW)	Depth (km)	M_w	strike	dip	rake	M_0 N-m	Location
04/03/83[a]	8.72	83.26	26	7.4	310	25	110	1.8 x10 20	Costa Rica (Osa)
03/25/90[b]	9.64	84.92	20	7.3	303	11	104	1.1 x10 20	Costa Rica (Nicoya)
04/22/91[c]	10.10	82.77	15	7.7	103	25	58	3.3 x10 20	Costa Rica (Limon)
09/02/92[d]	11.76	87.41	10	7.6	303	12	91	3.3 x10 20	Nicaragua

Geographical coordinates and depth from (a) *Adamek et al.* [1987], b,c *Protti et al.*, [1995, 1994], d USGS-NEIC. Seismic moment (M_0), moment magnitude (M_w) and other source parameters from Harvard CMT catalog. Strike and dip in degrees, strike measured clockwise from north. Rake (degrees) defined such that 90º represents pure reverse slip.

Table 5. Comparison of Geodetic and Geologic Characteristics of Osa and Nicoya

	Nicoya	Osa
Maximum locked slip on plate boundary[1]	5.6 cm/yr	7 cm/yr
Mean locked slip[1]	3.1 cm/yr	7 cm/yr
Fore arc shortening	No	Yes
Back arc deformation	No	Yes
Mean locked slip on plate boundary divided by plate rate[1,2]	36±3%	78±10%
High topography	No	Yes
Trench parallel block motion	Yes	No
Age of subducting sea floor	22-24 Ma	15-16 Ma
Bathymetry of subducted sea floor	Normal	Shallow (Cocos ridge)

1. For Osa, this is Cocos plate-Panama block motion, assuming 1 cm/yr shortening on Fila Costena

2. Calculated for depth range 10-50 km

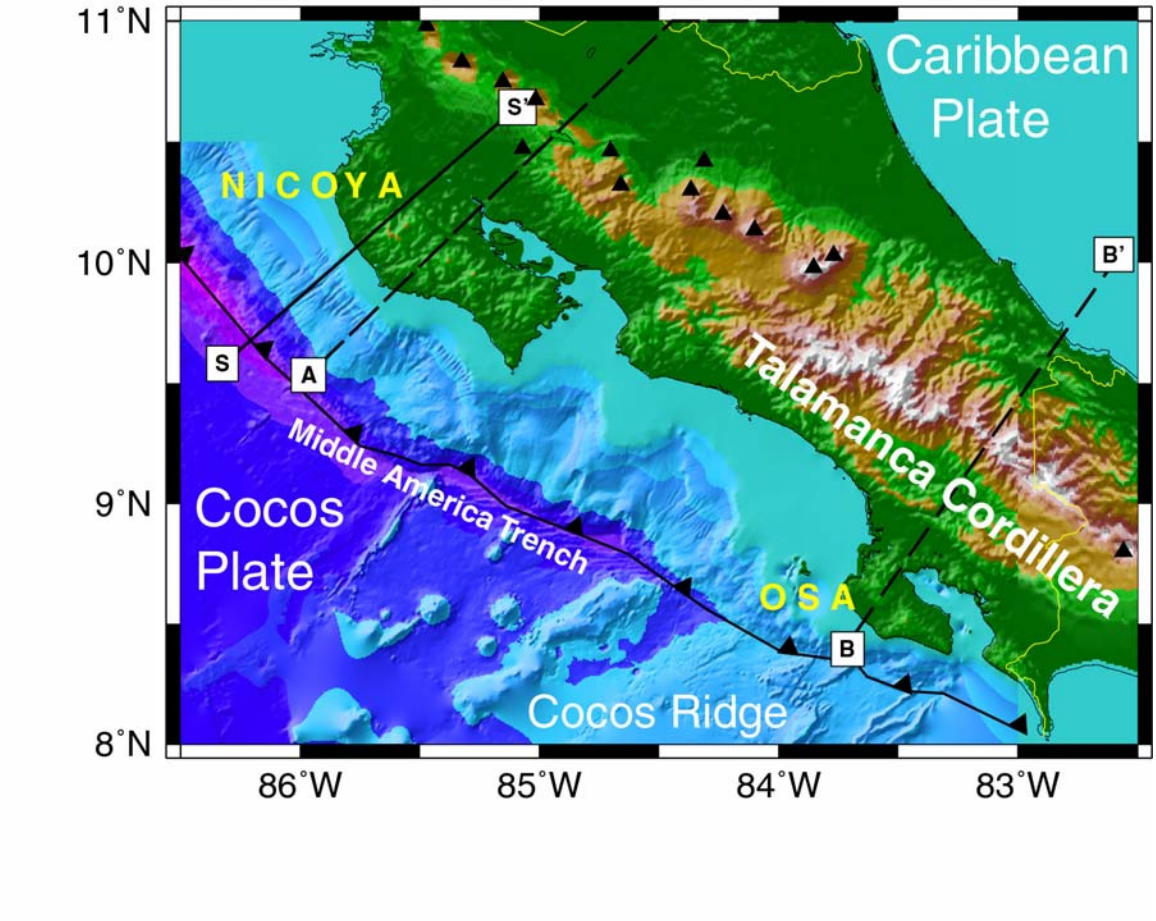

Figure 1. Location map with major physiographic and plate tectonic features of the study area. GN is Golfo Nicoya, GO is Golfo Osa, FC is Fila Costena, QP is Quepos Plateau. NPDB is North Panama Deformed Belt, part of the northern boundary of the Panama block (grey band). Volcanoes mentioned in text are Arenal (A), Tenorio (T) and Miravalles (M). Stars mark location of major earthquakes since 1980. White boxes outline areas shown in Figure 3a,b. Line S-S' shows location of seismic line 101 [*Christeson et al.*, 1999; *Sallarès et al.*, 2001] used in Figure 3c.

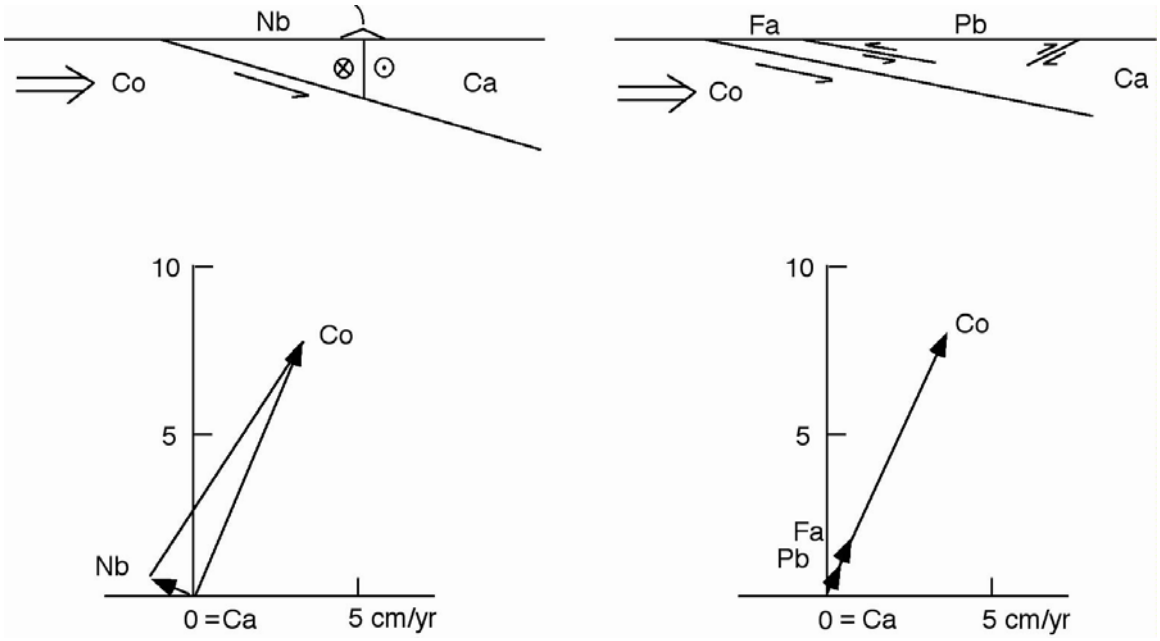

Figure 2. Cartoon comparing block tectonics for northern and southern Costa Rica. Top: cross-sections of plate and block convergence directions. Co is Cocos plate, Ca is Caribbean plate, Nb is Nicoya block, Pb is Panama block, Fa is fore-arc. Bottom: representative vector diagrams showing relative plate and block motions in a Caribbean plate reference frame.

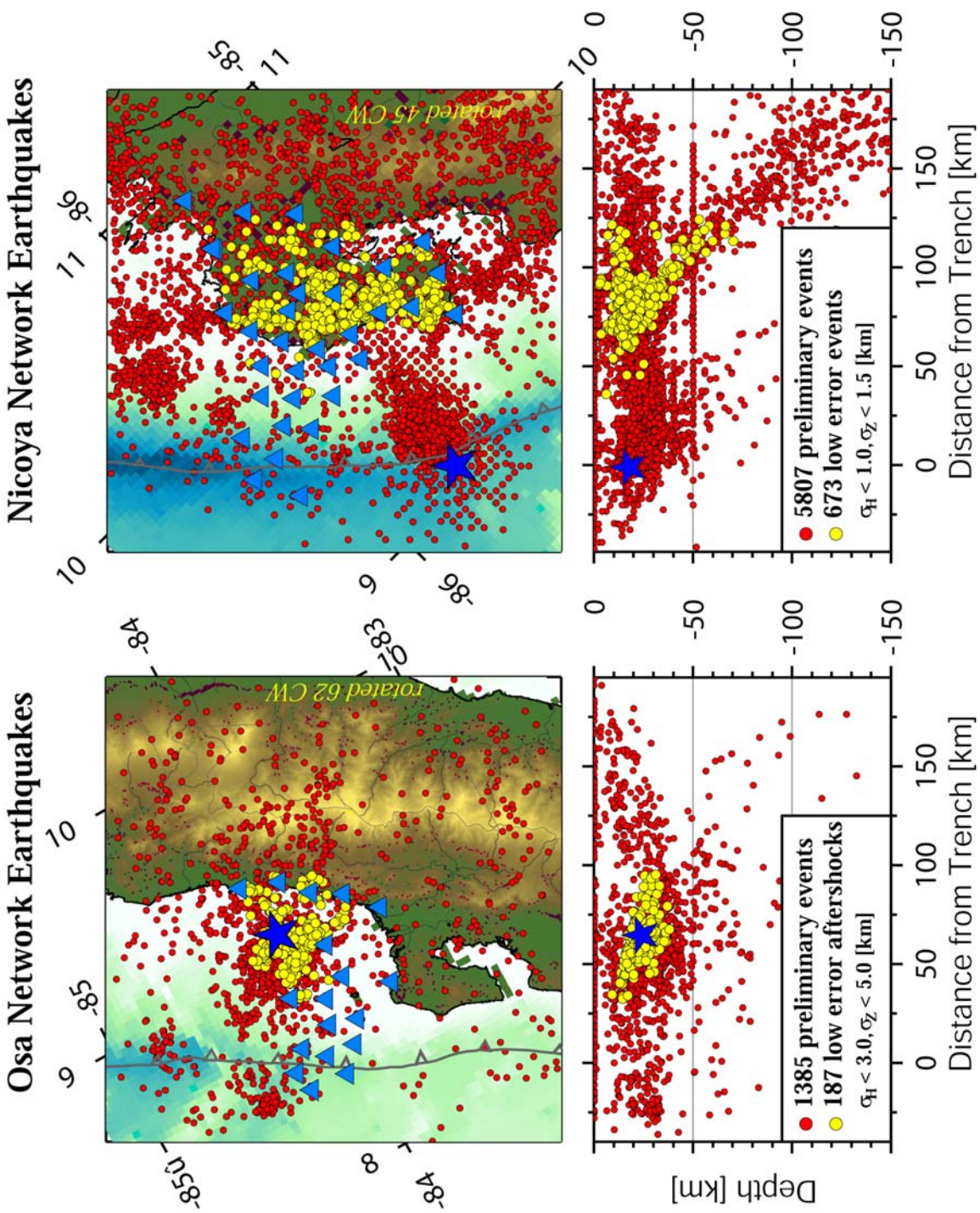

Figure 3a,b. Location of seismic instruments, and plan view and cross-section of earthquake locations, for Osa peninsula (a, left) and Nicoya peninsula (b, right). For Osa, star marks location of August 20, 1999 M_w 6.9 Quepos underthrusting earthquake. For Nicoya, star marks location of July 21, 2000 M_w 6.4 outer rise earthquake.

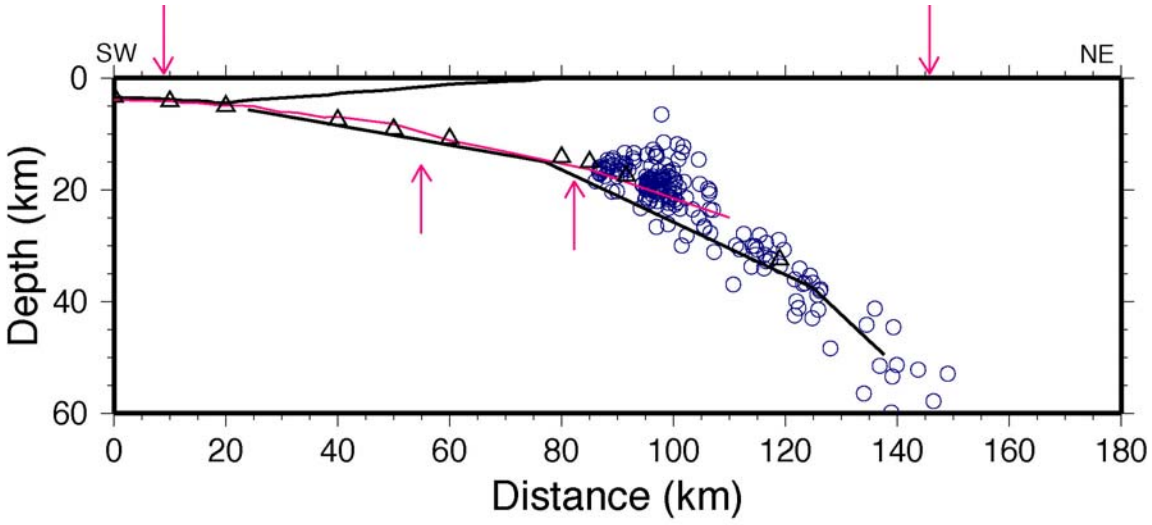

Figure 3c. Vertical cross section of plate boundary beneath Nicoya peninsula along profile S-S' (Figure 1): light solid line based on seismic refraction data of *Christeson et al.* [1999]; triangles based on re-analyses of these data by *Sallarès et al.* [2001]; circles are subset of well-located microearthquakes shown in Figure 2b (this study) within ±20 km of the profile, as recorded by OBS and land seismic arrays (with instruments located between downward pointing arrows at 10 km southwest of trench and 145 km northeast of trench); heavy solid line is plate boundary approximation used for GPS strain modeling. Plate boundary between upward pointing errors arrows 55 km and 80 km northeast of trench (11-18 km depth) is locked by amounts that exceed 50% of plate rate (see Figures 10 and 12).

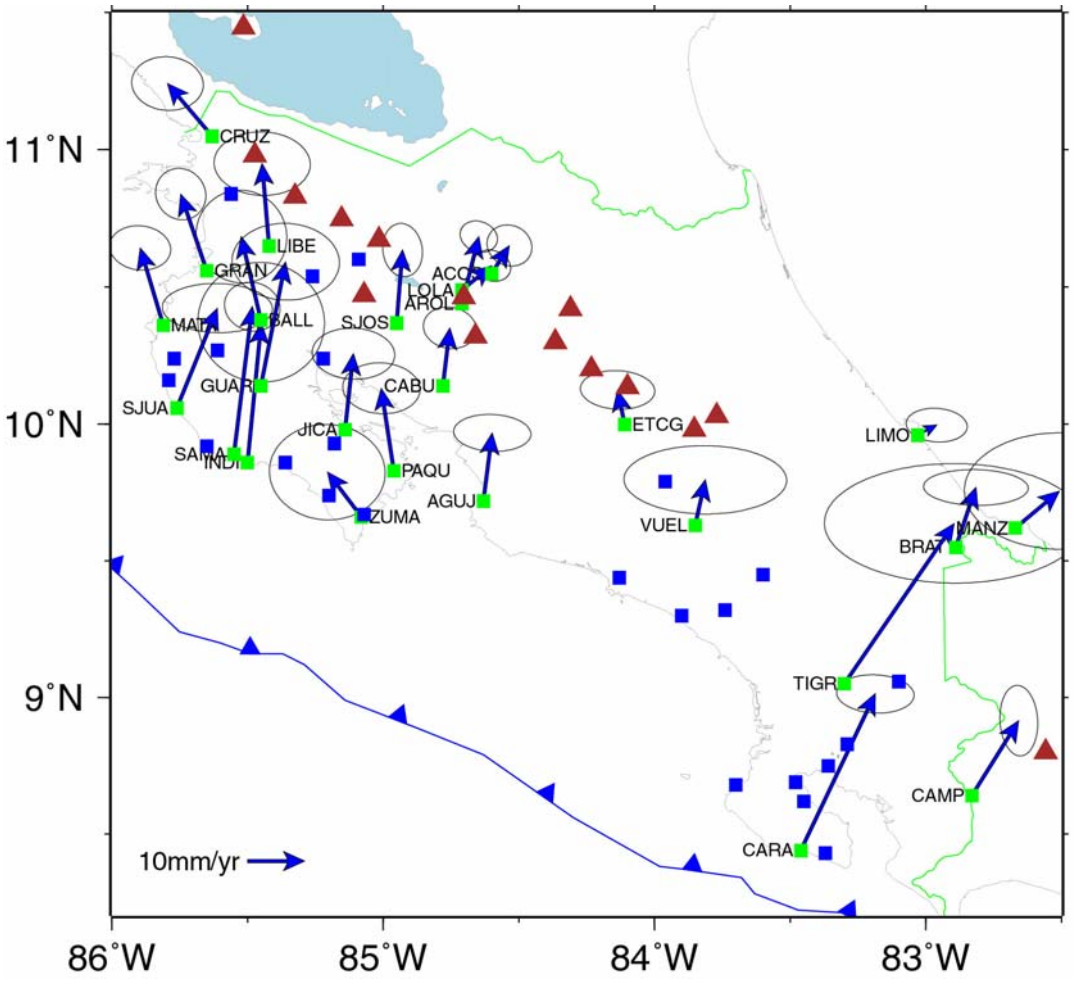

Figure 4. GPS site velocities with respect to the stable Caribbean plate: sites first occupied in 1994 are green squares with names, arrows show horizontal component of velocity vectors with 95% confidence ellipses; site first occupied in 2000 (velocities not yet defined) shown as blue squares. Red triangles are active volcanoes.

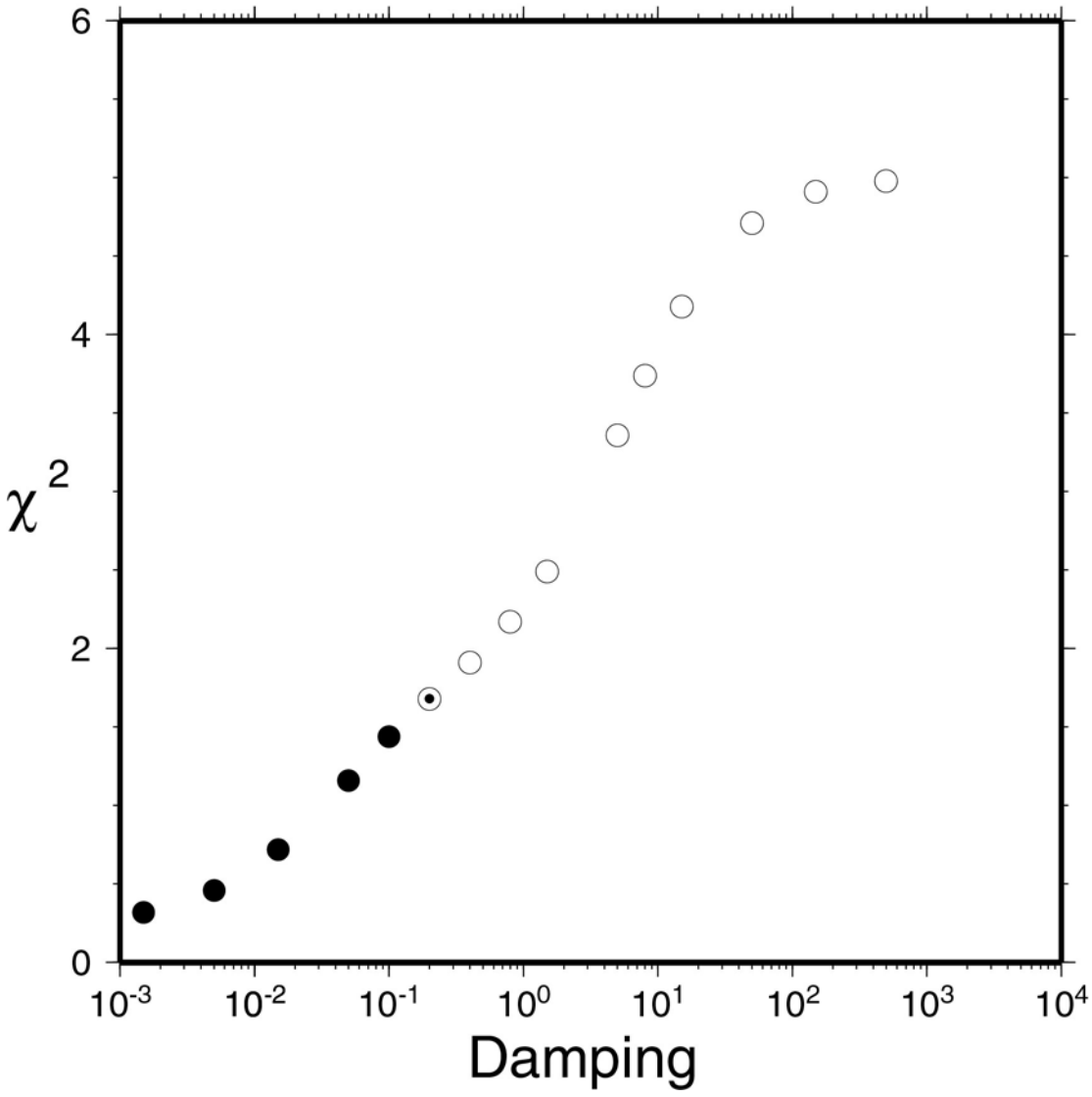

Figure 5. Typical trade-off curve (damping vs misfit, χ^2) for the inversion process. Largest damping value (10^3) gives uniform slip solution. Damping values smaller than 10^{-1} (solid circles) result in low misfit solutions but have negative slip on the fault plane, which may be physically unreasonable. Open circle with center dot represents damping value used for most results in this study.

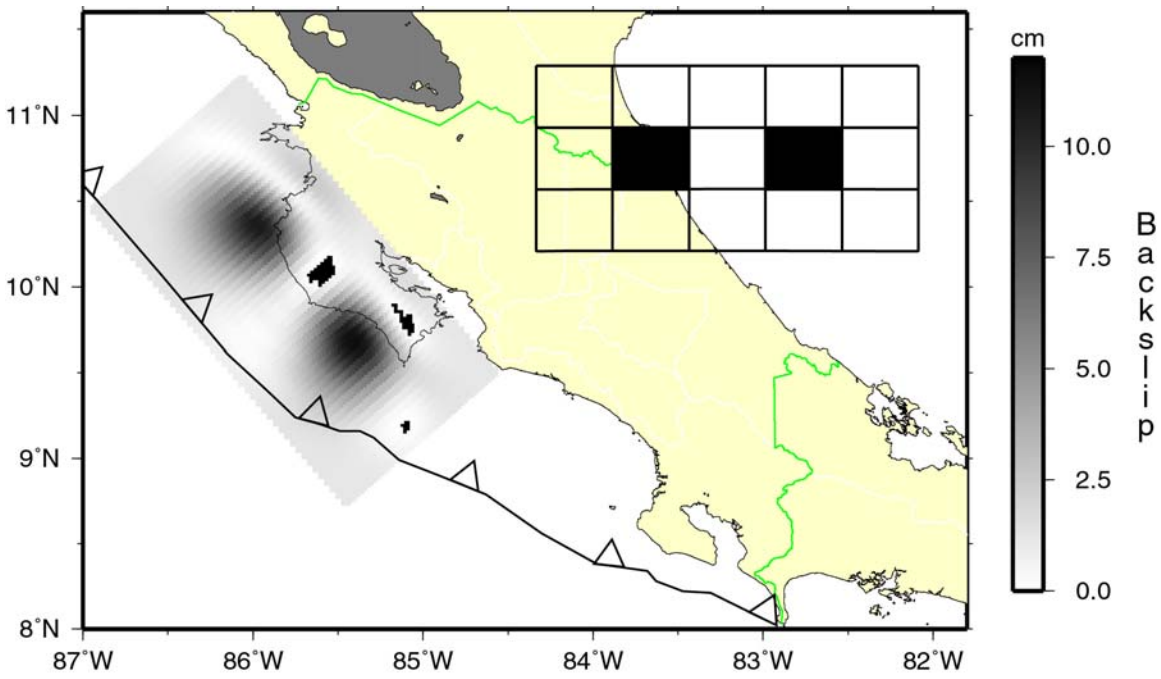

Figure 6. "Checkerboard" test for resolution of slip patches located offshore on main subduction thrust fault in the Nicoya area. Input slip distribution (displaced to upper right for clarity) consists of two locked patches, with 10 cm/yr of locked slip, surrounded by freely slipping zones. Output of inversion is shown in proper geographic position. Three small irregular black patches in output represent regions where inferred slip is negative.

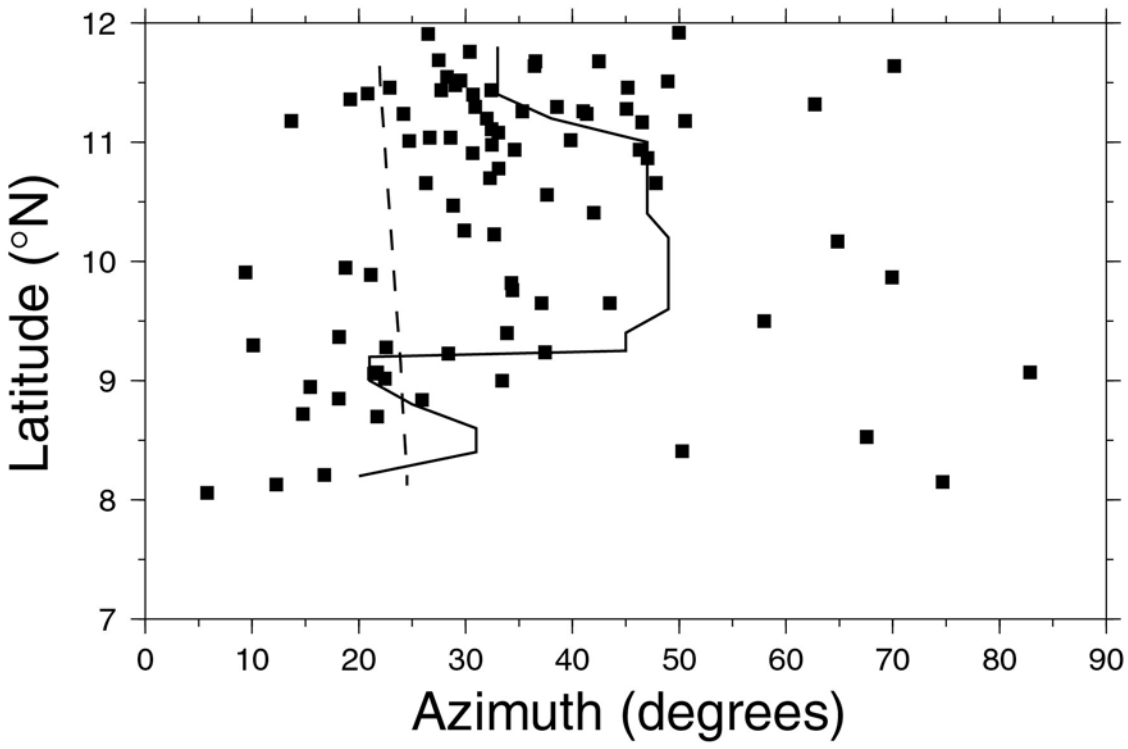

Figure 7. Azimuths of earthquake slip vectors for plate boundary events for Costa Rica and southern Nicaragua (solid squares), from the Harvard CMT catalog, compared to the azimuth of plate convergence (dashed line, from *DeMets* [2001]) and the trench-normal (solid line). South of about 9°N, the trench-normal and the convergence direction coincide (convergence orthogonal to the trench). Between 9°N and 11°N, plate convergence is about 20° oblique, and many earthquake slip vectors are intermediate between the convergence direction and the trench-normal.

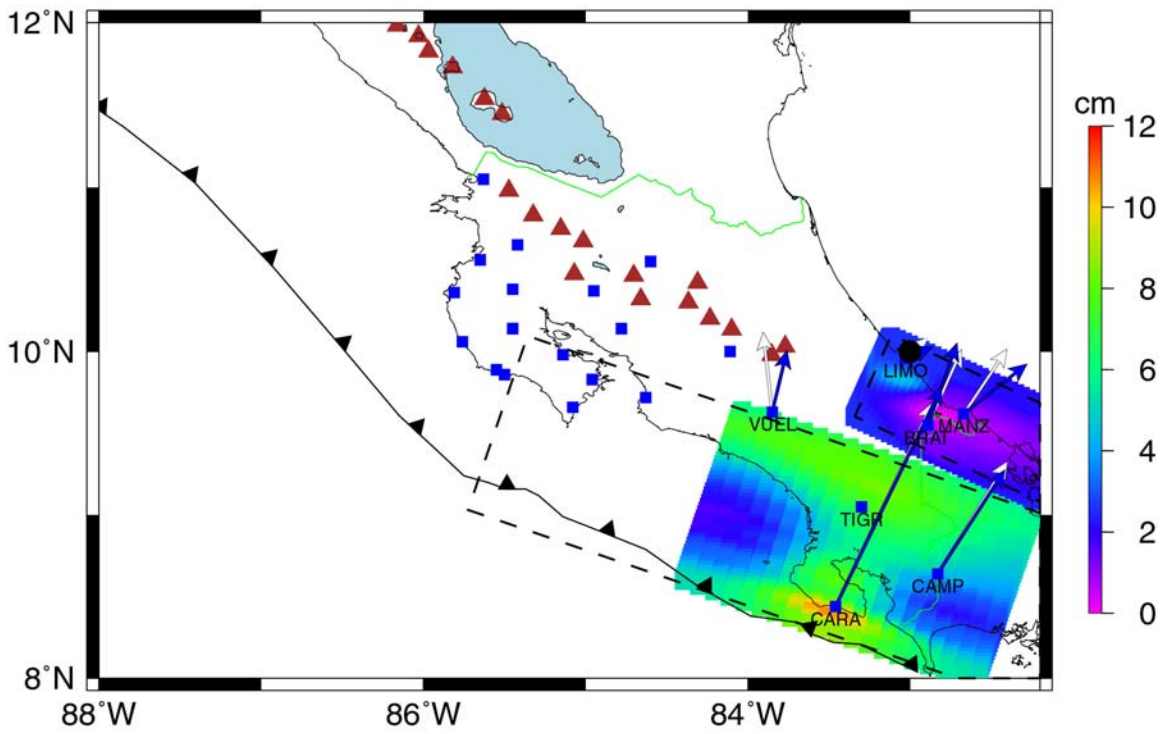

Figure 8. Best-fit model for locked slip in the Osa region. Red triangles are active volcanoes. Model fault planes (dashed lines) are colored in region where data density is sufficient for reliable results. Main plate boundary model plane (larger rectangle) extends northwest and southeast of data availability to avoid edge effects; back-arc plane extends only to southeast. Blue is calculated velocity at GPS site, white is observed. Patch of high locked slip near Pacific coast may be an artifact related to anomalously high velocity at site CARA.

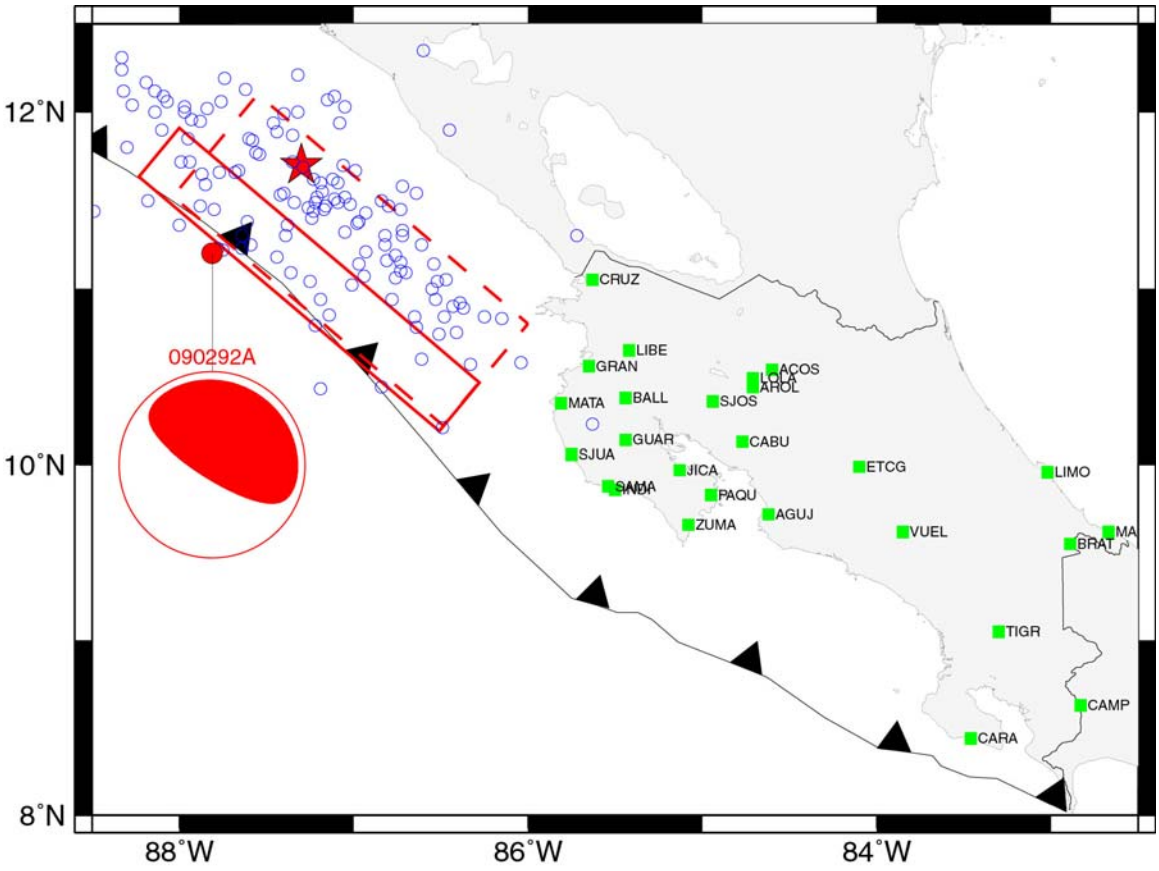

Figure 9. GPS site distribution in Costa Rica compared to rupture area of the 1992 Nicaragua tsunami earthquake. Star is earthquake epicenter (NEIC), representing location of initial rupture, estimated from first motion data. Solid circle is from Harvard CMT catalog, and represents location of maximum energy release (difference between these locations is consistent with slow up-dip rupture and tsunami generation). Small open circles are aftershocks from first 30 days (NEIC). Dashed rectangle is our estimate of rupture plane based on these aftershocks. Solid rectangle is rupture plane based on tsunami model [*Satake*, 1994a,b]. Sites in northern Costa Rica are near the southern part of the rupture area, regardless of how the rupture plane is defined.

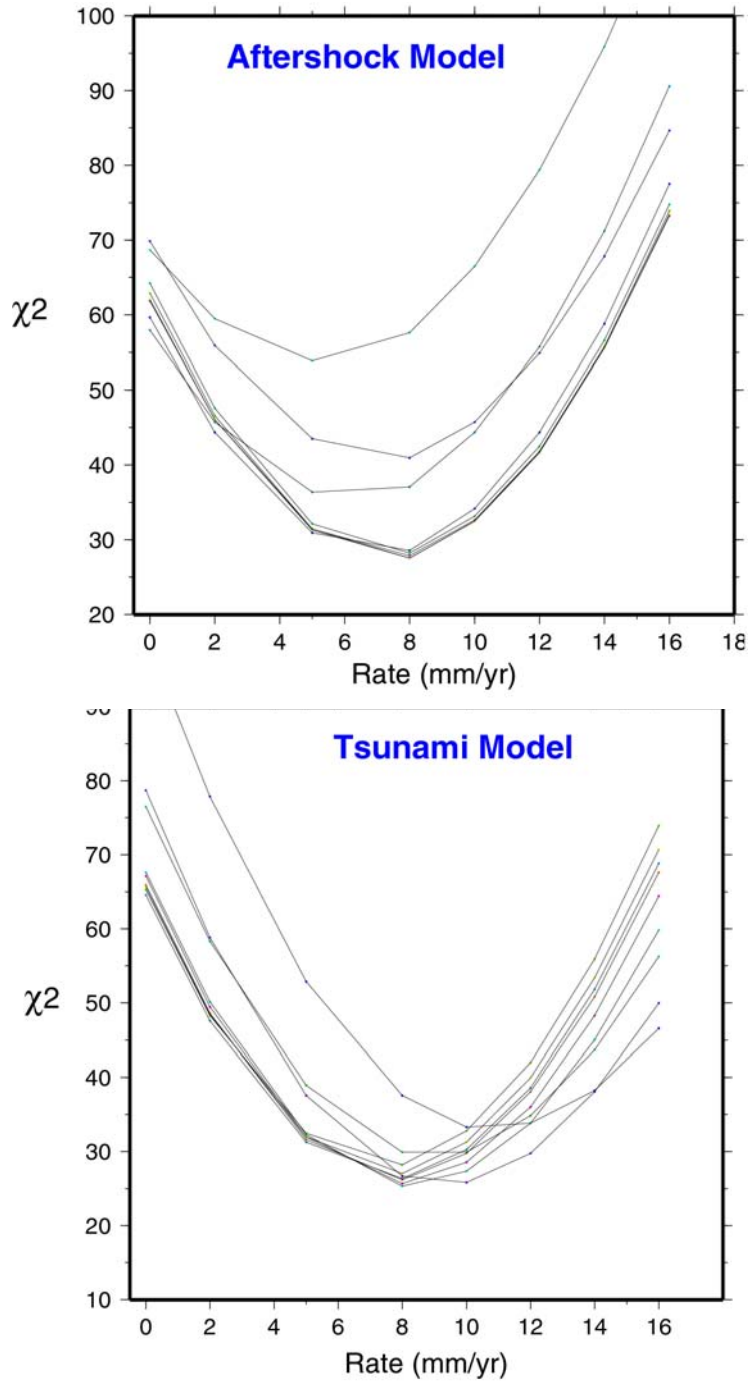

Figure 10. Misfit (χ^2) versus trench-parallel translation rate for the Nicoya block, for ten low misfit models of post-seismic response from the 1992 Nicaragua tsunami earthquake. a) fault plane defined by aftershocks, best fit model has viscosity of 10^{19} Pa-s (lower crust) and 10^{20} Pa s (upper mantle), fault slip 3-5 m; models with upper mantle viscosity of 10^{19} Pa s fit the data nearly as well. b) fault plane defined by tsunami model,

best fit model has viscosity of 10^{18} Pa-s (lower crust) and 10^{20} Pa s (upper mantle), fault slip 3 m; models with lower crust and upper mantle viscosity of 10^{18} and 10^{19} Pa s respectively and fault slip of 1m fit the data nearly as well.. There is a well-defined minimum at 8 mm/yr regardless of earthquake or rheological model. Uncertainty can be estimated by arbitrarily taking χ^2 value 10% larger than the minimum χ^2, giving ±3 mm/yr.

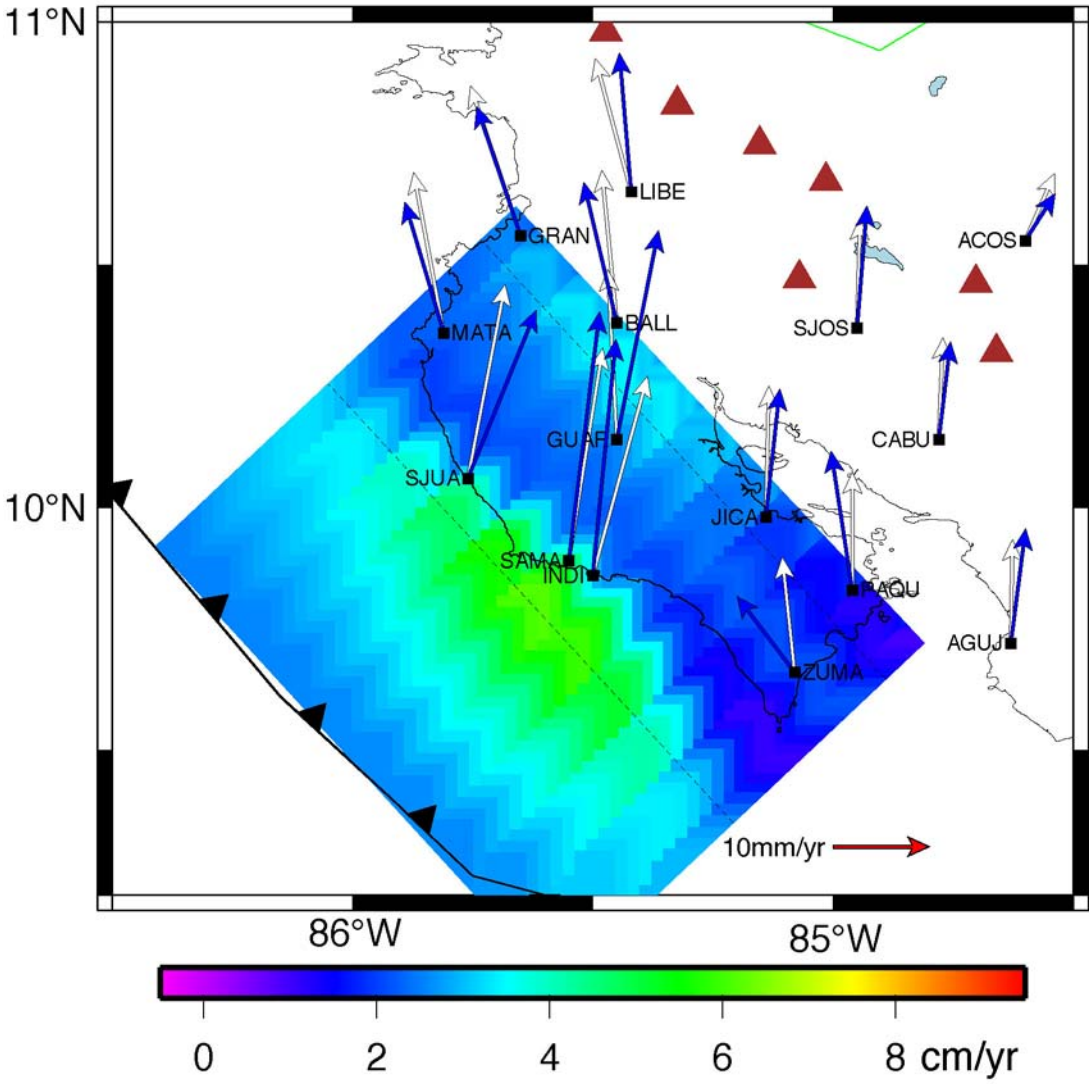

Figure 11. Best-fit model for locked slip on plate boundary, Nicoya region. Red triangles are active volcanoes. Light dashed lines parallel to trench show boundaries of three adjacent sub-planes in model plate boundary, with increasing dip to northeast (Figure 2c). Model planes are colored in region where data density is sufficient for reliable results, but extend northwest and southeast to avoid edge effects. Blue is calculated velocity at GPS site, white is observed. Note elliptical patch of high locked slip elongated parallel to the trench (maximum = 5.6 cm/yr) beneath the coastal area, and a second patch near the down-dip limit (maximum ~3 cm/yr).

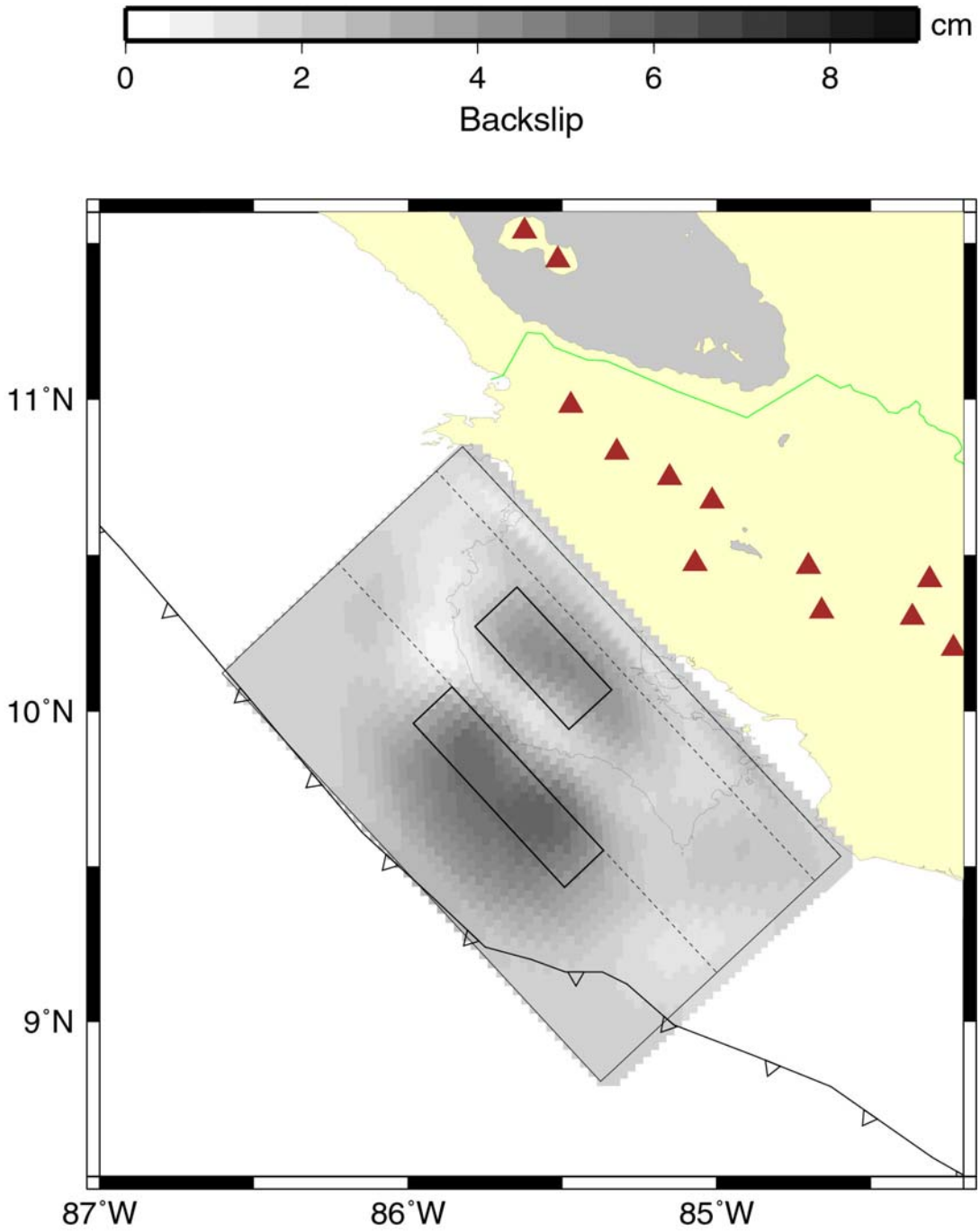

Figure 12. Checkerboard test to yield output similar to data inversion results. Rectangles outline areas of locked slip on plate boundary used as input to inversion (upper rectangle 20 by 80 km, 9 cm/yr of locked slip; lower rectangle 50 by 23 km, 4.5 cm/yr of locked slip); shading indicates output. Compare to Figure 10.

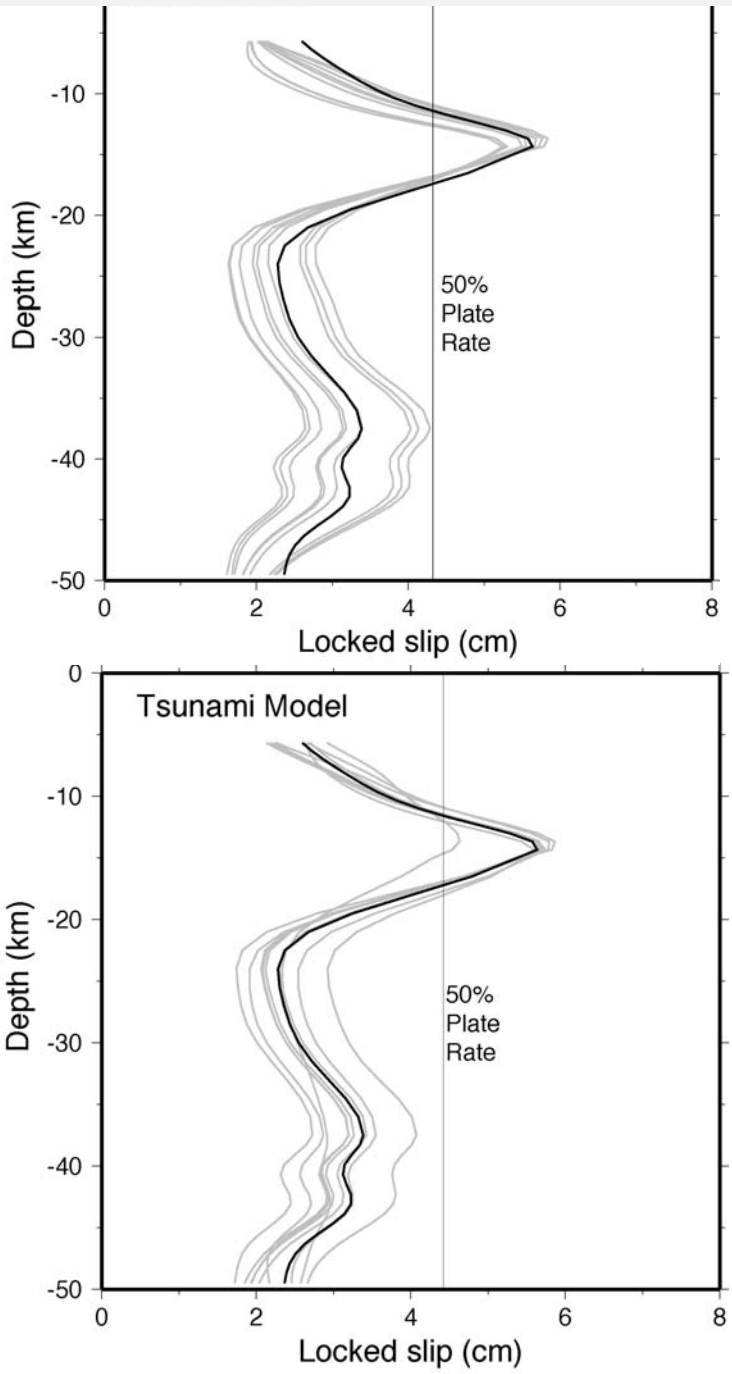

13. Locked slip on the plate boundary versus depth for the Nicoya region from inversions, for various models of post-seismic response from the 1992 Nicaragua tsunami earthquake (a, top: fault plane defined by aftershocks; b: fault plane defined by tsunami model; see Figure 8).

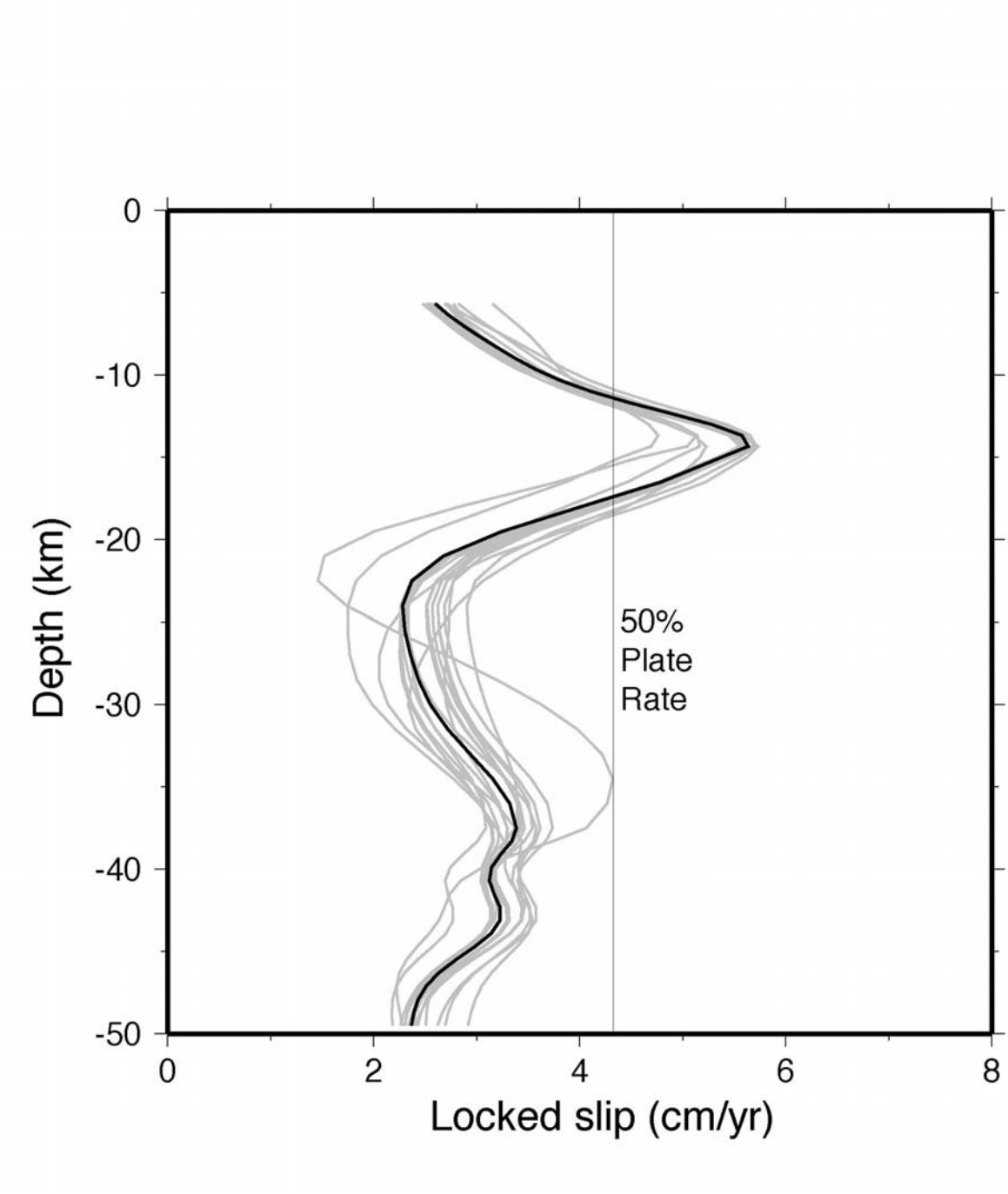

Figure 14. Similar to Figure 12, showing sensitivity of inversion results to blunders at individual GPS sites. Best fit post-seismic model and block translation rate are assumed. Successive data points in the Nicoya region are eliminated, and the data are re-inverted. For 17 starting data we perform 16 separate inversions using 16 data (thin grey lines) compared to best fit results using all 17 data (heavy solid line).

Figure 15. Variation in the location and magnitude of the deeper patch of locked slip as a function of the down-dip extent of the model plate interface, for three down-dip limits: 42 km, 50 km, 60 km.

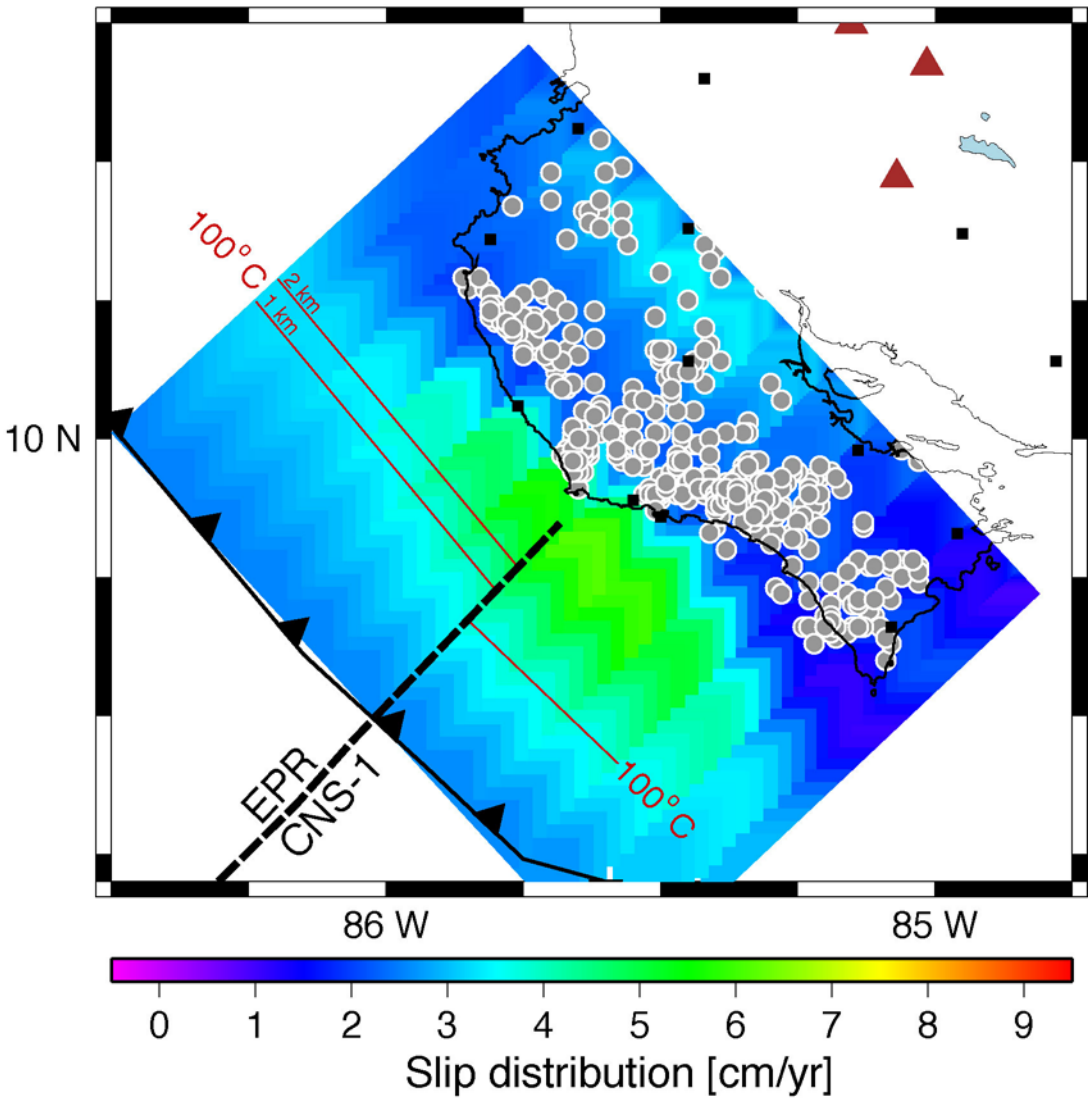

Figure 16. Comparison of well-located earthquakes from our seismic network, distribution of locked slip from inversion of the GPS data, and 100 °C isotherms from *Spinelli and Saffer* [2004] calculated assuming hydrothermal cooling of the upper 1 and 2 km of the EPR crust. Earthquakes reach an up-dip limit about 50 km from the trench; maximum locking (~6 cm/yr of locked slip) is centered about 35 km from the trench, approximately coincident with the 100°C isotherm that abruptly shallows across the boundary between crust generated at the East Pacific Rise (EPR) and Cocos-Nazca Spreading Center (CNS-1).

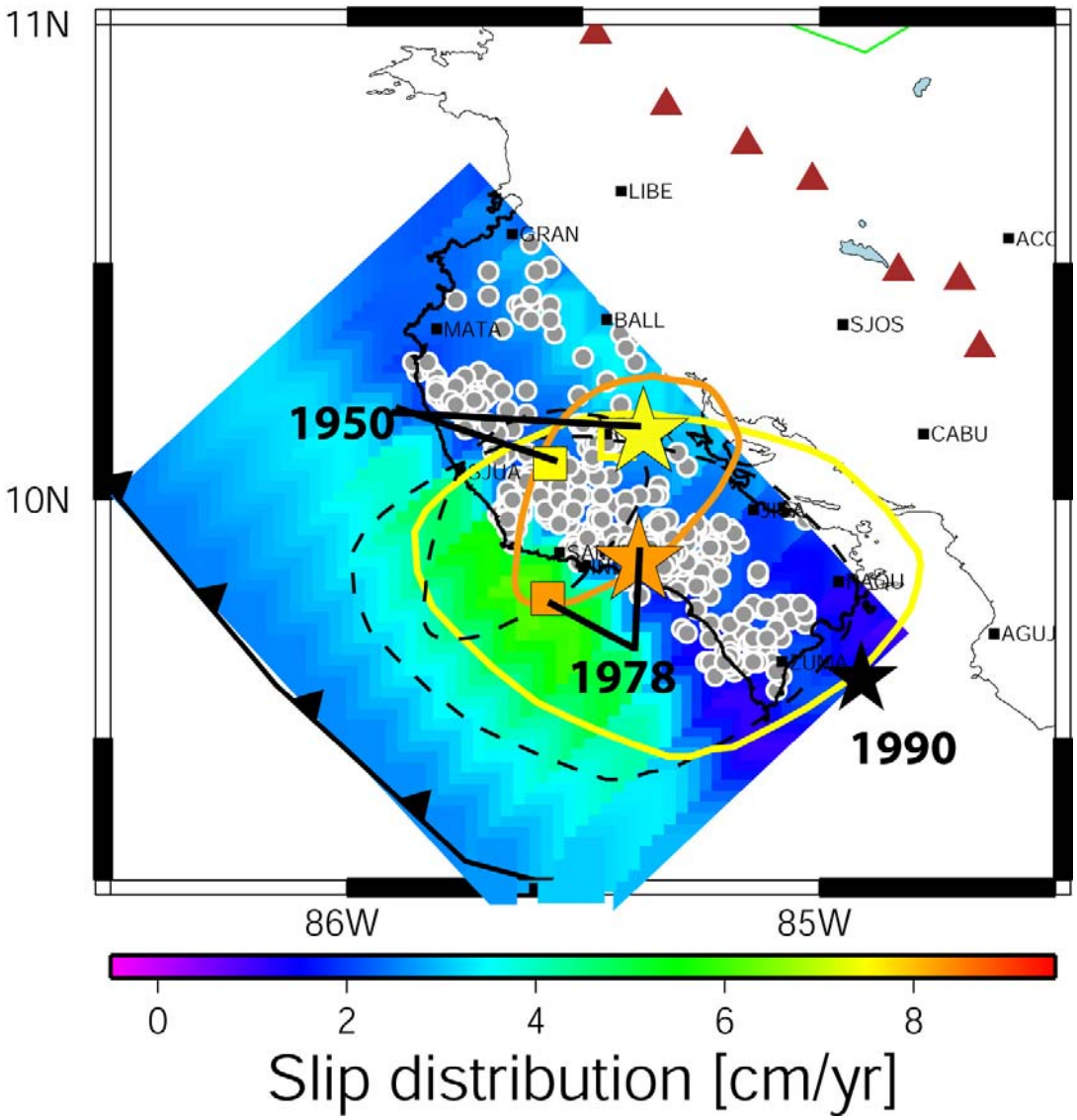

Figure 17. Original ISC (boxes) and relocated (stars) epicenters and corresponding rupture areas (dashed lines are original, colored solid lines are relocated) for the 1950 (Mw =7.7; yellow) and 1978 (Mw=7.0; orange) Nicoya earthquakes, superimposed on the distribution of locked slip from inversion of geodetic data. Epicenters and rupture areas are relocated relative to the well-located 1990 Mw=7.0 Gulf of Nicoya event (black star).

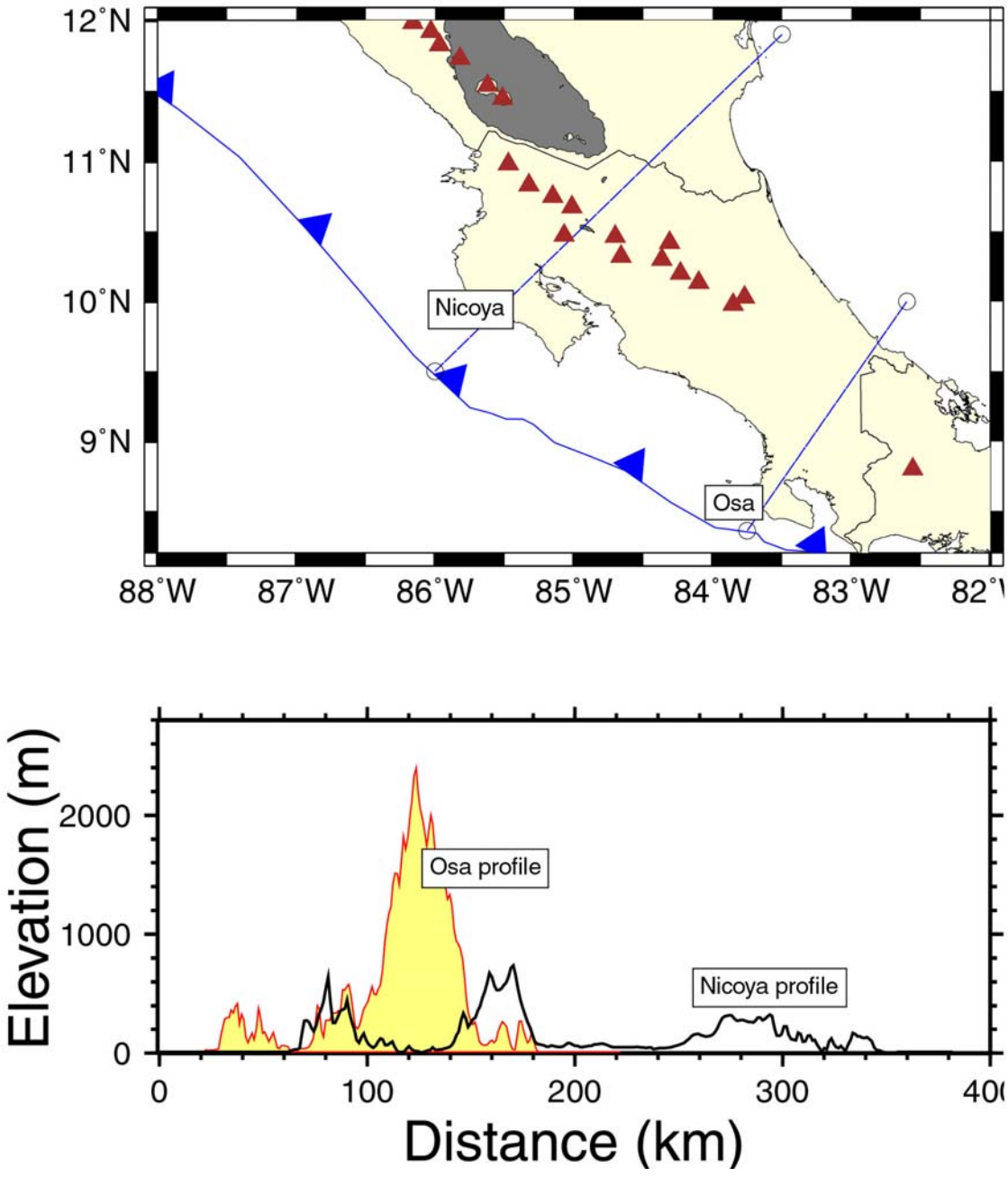

Figure 18. Topographic profiles for Osa and Nicoya.